NBR1 acts as an autophagy receptor for peroxisomes

Elizabeth Deosaran[1], Kenneth B. Larsen[2], Rong Hua[1,3], Graeme Sargent[1,3], Yuqing Wang[1,3], Sarah Kim[1], Trond Lamark[2], Miluska Jauregui[1], Kelsey Law[1,3], Jennifer Lippincott-Schwartz[4], Andreas Brech[5], Terje Johansen[2] and Peter K. Kim[1,3,*]

[1]Cell Biology Program, Hospital for Sick Children, Toronto, ON M5G 1X8, Canada
[2]Molecular Cancer Research Group, Institute of Medical Biology, University of Tromsø, 9037 Tromsø, Norway
[3]Department of Biochemistry, University of Toronto, Toronto, ON M5G 1X8, Canada
[4]Cell Biology and Metabolism Program, Eunice Kennedy Shriver National Institute of Child Health and Human Development, Bethesda, MD, USA
[5]Deptartment of Biochemistry, Institute for Cancer Research, Centre for Cancer Biomedicine, Oslo University Hospital, Oslo, Norway
*Author for correspondence (pkim@sickkids.ca)

Accepted 15 November 2012
Journal of Cell Science 126, 939–952

doi: 10.1242/jcs.114819

Summary

Selective macro-autophagy is an intracellular process by which large cytoplasmic materials are selectively sequestered and degraded in the lysosomes. Substrate selection is mediated by ubiquitylation and recruitment of ubiquitin-binding autophagic receptors such as p62, NBR1, NDP52 and Optineurin. Although it has been shown that these receptors act cooperatively to target some types of substrates to nascent autophagosomes, their precise roles are not well understood. We examined selective autophagic degradation of peroxisomes (pexophagy), and found that NBR1 is necessary and sufficient for pexophagy. Mutagenesis studies of NBR1 showed that the amphipathic α-helical J domain, the ubiquitin-associated (UBA) domain, the LC3-interacting region and the coiled-coil domain are necessary to mediate pexophagy. Strikingly, substrate selectivity is partly achieved by NBR1 itself by coincident binding of the J and UBA domains to peroxisomes. Although p62 is not required when NBR1 is in excess, its binding to NBR1 increases the efficiency of NBR1-mediated pexophagy. Together, these results suggest that NBR1 is the specific autophagy receptor for pexophagy.

Key words: Selective autophagy, Pexophagy, Autophagy receptors, NBR1, p62, Peroxisomes

Introduction

Peroxisomes are critical metabolic organelles that are required for oxidation of fatty acids, and reduction of hydrogen peroxide produced during lipid oxidation. They are required for synthesis of essential cellular components such as plasmalogens, isoprenoids and lysine. Unlike other metabolic organelles, peroxisome numbers are highly regulated, varying in numbers depending on cellular needs (Till et al., 2012). This plasticity is most readily observed in the liver of rodents. Upon activation of the nuclear receptor peroxisome proliferator-activated receptor-alpha (PPARα), peroxisome proliferation occurs by growth and division of pre-existing peroxisomes (Platta and Erdmann, 2007). However, upon removing the PPARα ligand, peroxisome numbers are quickly reduced to basal levels. This reduction is mediated by macro-autophagy, a catabolic mechanism of delivering large cytosolic material to lysosomes for degradation (Iwata et al., 2006). Little is known about the precise mechanism of macro-autophagy of peroxisomes, or macro-pexophagy (hereafter referred to as pexophagy). However, it is known that the inability to maintain peroxisome numbers is linked to various neurodegenerative and developmental disorders such as X-linked adrenoleukodystrophy, and Krabbe disease (Ribeiro et al., 2012; Singh et al., 2009). In particular, in some leukodystrophies, the loss of peroxisomes during neuroinflammation is thought to exacerbate the cellular inflammation, eventually leading to cell death (Kassmann and Nave, 2008).

Selective macro-autophagy (hereafter selective autophagy) is a catabolic cellular process by which large cytoplasmic materials are selectively sequestered and degraded in lysosomes. In the mammalian system, peroxisomes along with other cytosolic components such as protein aggregates, damaged mitochondria, ER, ribosomes, membrane remnants, midbody rings, intracellular bacteria, bacteriocidal precursor and viral capsid proteins are substrates of selective autophagy (reviewed by Johansen and Lamark, 2011; Kirkin et al., 2009b; Komatsu and Ichimura, 2010; Kraft et al., 2010). The mechanism of selective autophagy is not well understood. However, recent studies of various substrates are coalescing into a common theme in the mechanism of targeting selective substrates to autophagosomes. In this mechanism the substrate is activated for degradation by accumulation of ubiquitin (Ub) on the cytosolic side of the substrate followed by recruitment of ubiquitin-binding autophagy receptor(s) (Johansen and Lamark, 2011). The autophagy receptors play an essential role in linking the substrate to nascent autophagosomes by binding to both the ubiquitin on the substrate and the autophagy factor LC3 on the autophagosomes.

At present four Ub-binding mammalian autophagy receptors have been identified: p62, NBR1, NDP52 and optineurin (Bjørkøy et al., 2005; Kirkin et al., 2009a; Pankiv et al., 2007; Thurston et al., 2009; Wild et al., 2011). Recent studies suggest that depending on the substrate, these Ub-binding receptor proteins can either act cooperatively or independently. For example, both p62 and NBR1 have been reported to act cooperatively to target polyubiquitylated aggregates to autophagosomes (Kirkin et al., 2009a). However, *Salmonella* targeting to autophagosomes does not require NBR1, but instead

requires both p62 and NDP52 (Cemma et al., 2011; Zheng et al., 2009). These two autophagy receptors do not act cooperatively but appear to be recruited to *Salmonella* independently of each other. Similar results were observed for *Listeria*. However, for *Shigella* the recruitment of all three proteins was shown to be interdependent on each other (Mostowy et al., 2011).

The role of the various Ub-binding receptors in selective autophagy of organelles is not well understood. Several groups have reported that p62 is involved in mitophagy (the autophagic degradation of mitochondria); however, it is not clear whether p62 is required for targeting of ubiquitylated mitochondria to autophagosomes or serves a different functional role (Ding et al., 2010; Geisler et al., 2010; Narendra et al., 2010; Okatsu et al., 2010). Recently, we showed that p62 is involved in selective degradation of peroxisomes when peroxisomes were labeled with ubiquitin (Kim et al., 2008). Depleting cells of p62 using siRNA resulted in a decrease in peroxisome turnover, thus causing an increase in peroxisome numbers. However, the role of NBR1 in pexophagy is not known.

Here, we tested the hypothesis that autophagy receptors confer substrate selectivity in autophagy. For these studies we used peroxisomes as substrates for selective autophagy and examined the role of two autophagy receptors, NBR1 and p62. Peroxisomes were selected as the substrate to examine the role of these two receptors for two reasons. First, peroxisome numbers can be readily quantified, allowing for monitoring changes in their numbers both statically and dynamically. Second, except for our previous report implicating p62 in the clearance of peroxisomes (Kim et al., 2008), little is known about the role of other autophagy receptors, like NBR1, in mammalian pexophagy. Here, we characterize the roles of both NBR1 and p62 in targeting of peroxisomes to autophagosomes for their degradation. Based on our findings we present a mechanism for substrate specificity in selective autophagy. NBR1 uses a mechanism similar to 'coincidence detection', where the combination of the ubiquitin-binding UBA domain and the phospholipid-binding J domain functions as an effective 'coincidence detector' (Carlton and Cullen, 2005), allowing NBR1 to target peroxisomes for autophagic degradation.

Results

NBR1 is required for the turnover of peroxisomes

Recently, NBR1 and p62 were shown to act together to selectively target polyubiquitylated protein aggregates to autophagosomes for degradation (Kirkin et al., 2009a). p62 was also shown to be involved in pexophagy (Kim et al., 2008). However, it is not known whether NBR1 is required for peroxisome degradation, and if so, whether it works cooperatively with p62. In order to address this question, we depleted HeLa cells of NBR1 using siRNA and examined whether its loss affected the endogenous level of peroxisomes. To quantify the change in peroxisome numbers, the total fluorescence intensity from a peroxisomal protein, catalase, was quantified by indirect immunofluorescence (Huang et al., 2011; Kim et al., 2008). To ensure that only cells with knockdown of p62 and/or NBR1 were quantified, they were co-immunostained for p62 and/or NBR1 expression.

As shown previously (Kim et al., 2008), knocking down p62 expression resulted in an increase in catalase levels relative to the cells treated with non-targeting siRNA, suggesting that p62 depletion inhibited the endogenous turnover of peroxisomes (Fig. 1A,B). Similarly, in cells where NBR1 was depleted, an increase in catalase levels was also observed, suggesting that NBR1 is also involved in the endogenous turnover of peroxisomes (Fig. 1A,B). The increase in peroxisomal catalase levels in p62 and NBR1 knockdown cells was confirmed by western blot analysis, which showed elevated catalase levels in cells where either NBR1 or p62 was depleted (Fig. 1C). We also examined the autophagy receptor NDP52, which was previously shown to be involved in autophagy of the bacterial pathogen *Salmonella typhimurium* (Thurston et al., 2009). When NDP52 expression was knocked down using siRNA, the endogenous level of peroxisomes was not affected (supplementary material Fig. S1). Hence, NDP52 is not required for basal peroxisome turnover. Together, these experiments suggest that NBR1 and

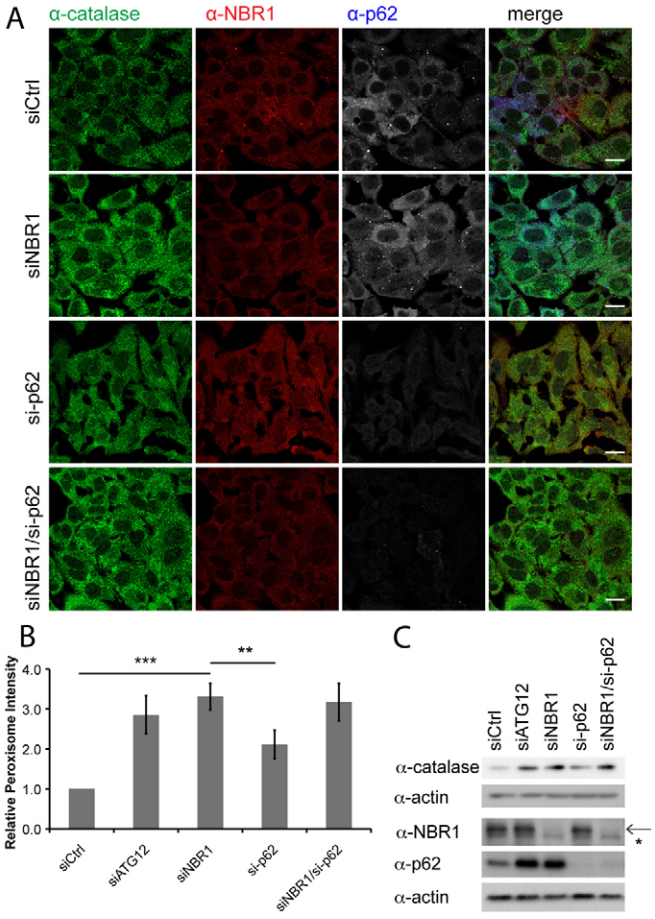

Fig. 1. NBR1 is required for pexophagy. (**A**) HeLa cells were transfected with non-targeting siRNA (siCtrl), siRNA against p62, NBR1, or against both p62 and NBR1, as indicated, over two consecutive days. Two days later, the cells were fixed and immunostained for catalase, NBR1 and p62. Scale bars: 10 μm. (**B**) The normalized mean fluorescence intensity of catalase levels of at least 100 cells in A. The average ($n=3$) for each condition was normalized against the control non-targeting siRNA (siCtrl). Only cells showing a decrease in NBR1 and/or p62 expression were quantified, with the exception of the control experiment. Error bars indicate s.d. ***$P<0.001$, **$P=0.001$–0.01. (**C**) Total cell lysates were prepared from siRNA-treated cells (as in A) and immunoblotted with catalase, NBR1, p62 and actin antibodies. In the NBR1 blot, two bands are present. The arrow indicates the NBR1 band and the asterisk indicates a cross-reacting band.

p62, but not NDP52, are required for basal turnover of peroxisomes.

NBR1 and p62 act in the same pathway

Interestingly, the increase in catalase levels in NBR1 knockdown cells was significantly higher than those observed in p62 knockdown cells (Fig. 1B,C). A possible explanation for this observation is that p62 and NBR1 mediate independent but parallel peroxisome degradation pathways, like that found with NDP52 and p62 in *S. typhimurium* (Cemma et al., 2011). Conversely, both may be involved in the same pathway but at different stages. To determine whether p62 and NBR1 act in two distinct parallel pathways, we knocked down the expression of both p62 and NBR1 simultaneously and quantified peroxisomal catalase levels (Fig. 1B). If NBR1 and p62 are involved in different but parallel pathways, depletion of both proteins should result in an additive increase in peroxisome levels. If NBR1 and p62 are involved in the same pathway but at different steps, then no additive increase should be observed when both proteins are depleted. As shown in Fig. 1B, when both NBR1 and p62 were knocked down, the increase in peroxisome levels was not additive but remained similar to NBR1-only knockdown conditions. This result was further verified by western blot of endogenous catalase levels that showed no further increase in catalase upon knockdown of both p62 and NBR1 compared to NBR1 alone (Fig. 1C). Thus, NBR1 and p62 act in the same pathway.

Exogenously expressed NBR1 induces peroxisome clustering

If p62 and NBR1 are involved in the same pathway, they may function cooperatively to target peroxisomes to autophagosomes, similarly to polyubiquitylated protein aggregates. If this is the case, then the differential inhibition of pexophagy observed between NBR1 and p62 knockdown conditions (Fig. 1B) suggests that NBR1 may play the initiating or prominent role in mediating pexophagy. This hypothesis is supported by the observation that knockdown of NBR1 resulted in a similar increase in catalase levels compared to cells where autophagy was inhibited by knockdown of the autophagic factor ATG12 (Fig. 1B,C; supplementary material Fig S2). A possible explanation for these results is that NBR1 may be recruited to peroxisomes to activate the targeting of peroxisomes to autophagosomes before p62. If this model is true, then overexpression of NBR1 should upregulate pexophagy by increasing the amount of free NBR1 that can bind to peroxisomes.

We tested this hypothesis by first asking whether exogenously expressed NBR1 colocalized with endogenous peroxisomes. Peroxisomes were identified using antibodies against endogenous catalase or PMP70 (Fig. 2A,F). When we expressed a Cherry–NBR1 chimera protein, we observed that peroxisomes clustered around NBR1-positive punctate structures (Fig. 2B,C). Peroxisome clustering was not observed in cells expressing Cherry–p62 (Fig. 2D,E). In order to illustrate the differences in peroxisome binding between the two autophagy receptors, we quantified the Manders' colocalization coefficient of Cherry signal overlapping with catalase/PMP70 (M_{Cherry}) for both autophagy receptors. For these quantifications, only cells with similar expression levels (as determined by the total Cherry fluorescence in each cell) were quantified. In comparison to Cherry–p62, Cherry–NBR1 showed a significantly higher colocalization coefficient with endogenous catalase and PMP70 (Fig. 2G). Similar NBR1/peroxisome clusters were observed in other cell lines, such as COS7, HEK293 and wild-type mouse embryonic fibroblasts (MEFs), showing that the observed phenomenon was not cell type specific (data not shown).

To determine the nature of these NBR1/peroxisome clusters, we examined HeLa cells expressing NBR1 by correlative light–electron microscopy (CLEM). As seen in the representative images (Fig. 3A–D), we found two populations of NBR1-positive structures. One group consisted of clusters of single membrane vesicular-like structures with a diameter of 40–70 nm (Fig. 3D, arrow). The second population clearly shows these vesicular-like structures sequestered within a double-membrane structure resembling typical autophagosomes (Fig. 3D, arrowhead). The identity of these NBR1 clusters was further verified by immuno-EM on cells transfected with GFP-NBR1 (Fig. 3E). To establish the relationship between these NBR1 vesicle structures and peroxisomes, we transfected HeLa cells with Cherry–NBR1 and the peroxisomal marker GFP–PMP34 (Fig. 3F–H). At high magnification we observed many peroxisome-like vesicles, often localized at the periphery of the aggregates (Fig. 3I,K). These results confirm the clustering of peroxisomes with NBR1 observed by confocal fluorescence microscopy.

NBR1 promotes targeting of peroxisomes to lysosomes

To determine whether the peroxisome/NBR1 clusters lead to targeting of peroxisomes to lysosomes we looked for colocalization with the lysosomal marker Lamp1 (supplementary material Fig. S3). To prevent degradation of peroxisomes and NBR1 within lysosomes, and allow their visualization, cells were treated with the lysosomal protease inhibitors E-64 and leupeptin. The majority of the NBR1 punctate structures colocalized with Lamp1 (supplementary material Fig. S3A). This colocalization was abolished upon treating the cells with the autophagy inhibitor 3-methyladenine (3-MA) (supplementary material Fig. S3B), suggesting that the colocalization of NBR1 with lysosomes was mediated by autophagy. We also examined whether peroxisome/NBR1 clusters also colocalized with lysosomes. When Cherry–NBR1/Lamp1–GFP-expressing cells were probed for endogenous catalase, the majority of peroxisomes were found clustered with NBR1 within lysosomes (supplementary material Fig. S3C–E). To determine the extent of this clustering we quantified the number of the NBR1/peroxisome clusters that colocalized with the lysosomal marker Lamp1. In these cells 85±13% of these clusters were found inside lysosomes. However, there was a small population of cells (~10%) that had large NBR1 aggregates with peroxisomes clustered around them but not localized inside lysosomes. The other 5% on average did not colocalize with peroxisomes. Time-lapse imaging of cells expressing Cherry–NBR1 and the peroxisomal marker PMP34-GFP verified that peroxisomes were targeted to lysosomes for degradation when NBR1 was overexpressed. As the expression of NBR1 increased, peroxisomes clustered around NBR1, and eventually disappeared (supplementary material Movie 1). Next we asked whether NBR1/peroxisome clusters localize with autophagosomes. In cells expressing GFP–NBR1 along with the autophagosome marker Cherry–LC3 we found that NBR1/peroxisome clusters colocalized with Cherry–LC3-positive structures (supplementary material Fig. S3F,G). Together, these

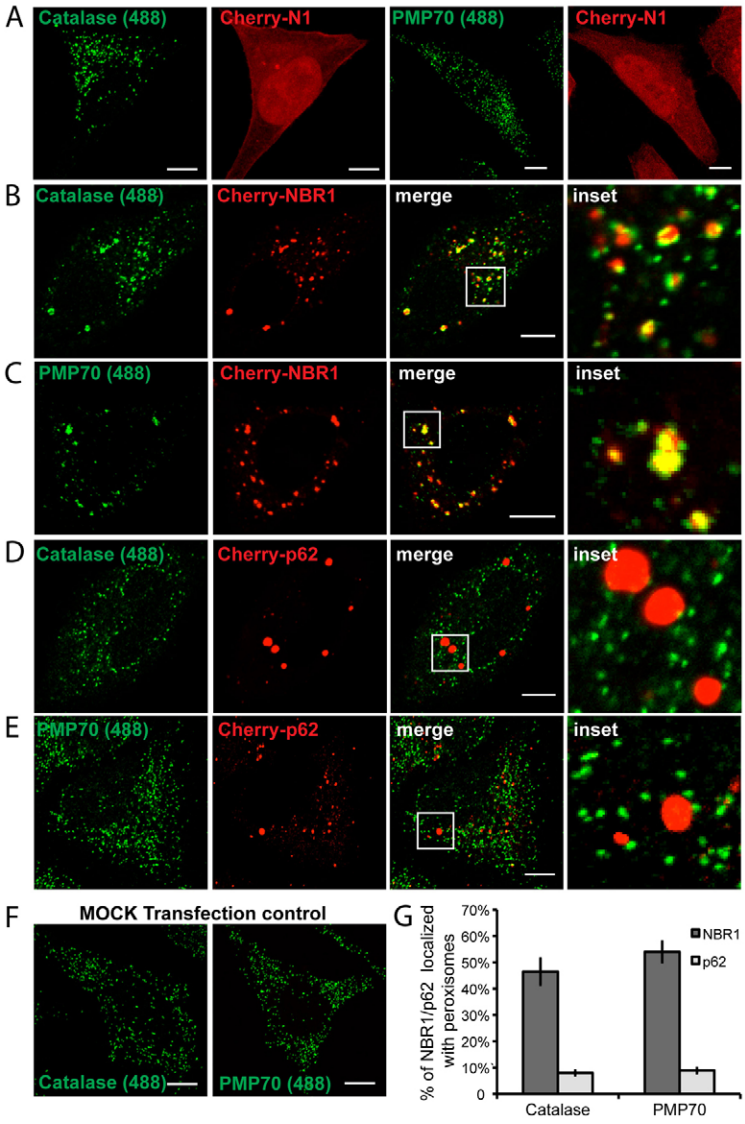

Fig. 2. Exogenously expressed NBR1 promotes peroxisome clustering and targeting to lysosomes. (**A**) HeLa cells transfected with Cherry-N1 and immunostained for either catalase or PMP70 as indicated. (**B**,**C**) A representative image of HeLa cells transiently transfected with Cherry-NBR1 and immunostained for endogenous catalase (B), or PMP70 (C). (**D**,**E**) Cells were transiently transfected with Cherry-p62 and immunostained for catalase (D) or PMP70 (E). Also shown on the right in B–E are enlarged images of the boxed regions in the merge panels. (**F**) Mock-transfected HeLa cells immunostained for either catalase or PMP70. (**G**) Bar graph of the percentage of Cherry–NBR1 or Cherry–p62 colocalized with either endogenous catalase or PMP70, as indicated. Percentage colocalization was determined by calculating Manders' colocalization coefficient. At least 50 cells were quantified for each set of three independent experiments. Error bars indicate s.d. All images are single confocal images. Scale bars: 10 μm.

results strongly suggest that exogenously expressing NBR1 causes an increased targeting of peroxisomes to lysosomes by autophagy.

In order to visualize and quantify pexophagy activity due to elevated NBR1 levels, we employed a pH-sensitive live-cell assay hereafter referred to as the 'RG-lysosome assay' (Pankiv et al., 2007). In this assay a tandem chimera of mCherry and EGFP fused to the peroxisome membrane targeting sequence of PEX26 (GFP–Cherry–PEX26$_{TM}$) is expressed in HeLa cells. Since the fluorescence of mCherry is more acid resistant than EGFP, peroxisomes targeted to lysosomes maintain their red fluorescent signal while the GFP fluorescence gets quenched. Thus, GFP–Cherry–PEX26$_{TM}$ localized inside lysosomes exhibits red fluorescence only, while cytoplasmic protein appears yellow due to the combination of red and green fluorescence (supplementary material Fig. S4). Time lapse imaging of cells expressing Cer–NBR1 and GFP–Cherry–PEX26$_{TM}$ over 2 days revealed an NBR1-mediated gradual movement of peroxisomes into lysosomes, followed by disappearance of peroxisomes (supplementary material Movie 2). The disappearance of peroxisomes was preceded by an increase in 'Red' peroxisomes (which appear slightly purple due to overlap with the blue signal from Cer–NBR1). Unlike GFP, Cerulean has a low pK_a (4.7), thus it maintains its fluorescence signal within the low pH environment of lysosomes (Rizzo et al., 2004).

In order to assess the ability of exogenously expressed NBR1 to induce pexophagy we quantified pexophagy using the RG-lysosome assay in cells coexpressing GFP–Cherry–PEX26$_{TM}$ with Cer–NBR1, Cer–p62 or Cerulean (Cer). We considered a cell to show increased pexophagy if 20% or more of its total Cherry pixels were 'red-only' (supplementary material Fig. S4). A pixel was considered to be 'red-only' if the fluorescent signal from Cherry was at least three times higher than the GFP signal (see Materials and Methods). There was a significant increase in the number of cells with elevated pexophagy upon expressing Cer–NBR1 compared to Cer–p62 or Cerulean alone (Fig. 4A,B). Interestingly, no significant difference was observed between cells expressing Cer–p62 compared to Cerulean alone (Fig. 4B). To demonstrate that the increase in the red-only signal was due to pexophagy, we treated the cells with 3-MA and found that it prevented the accumulation of red-only signal (Fig. 4A,B).

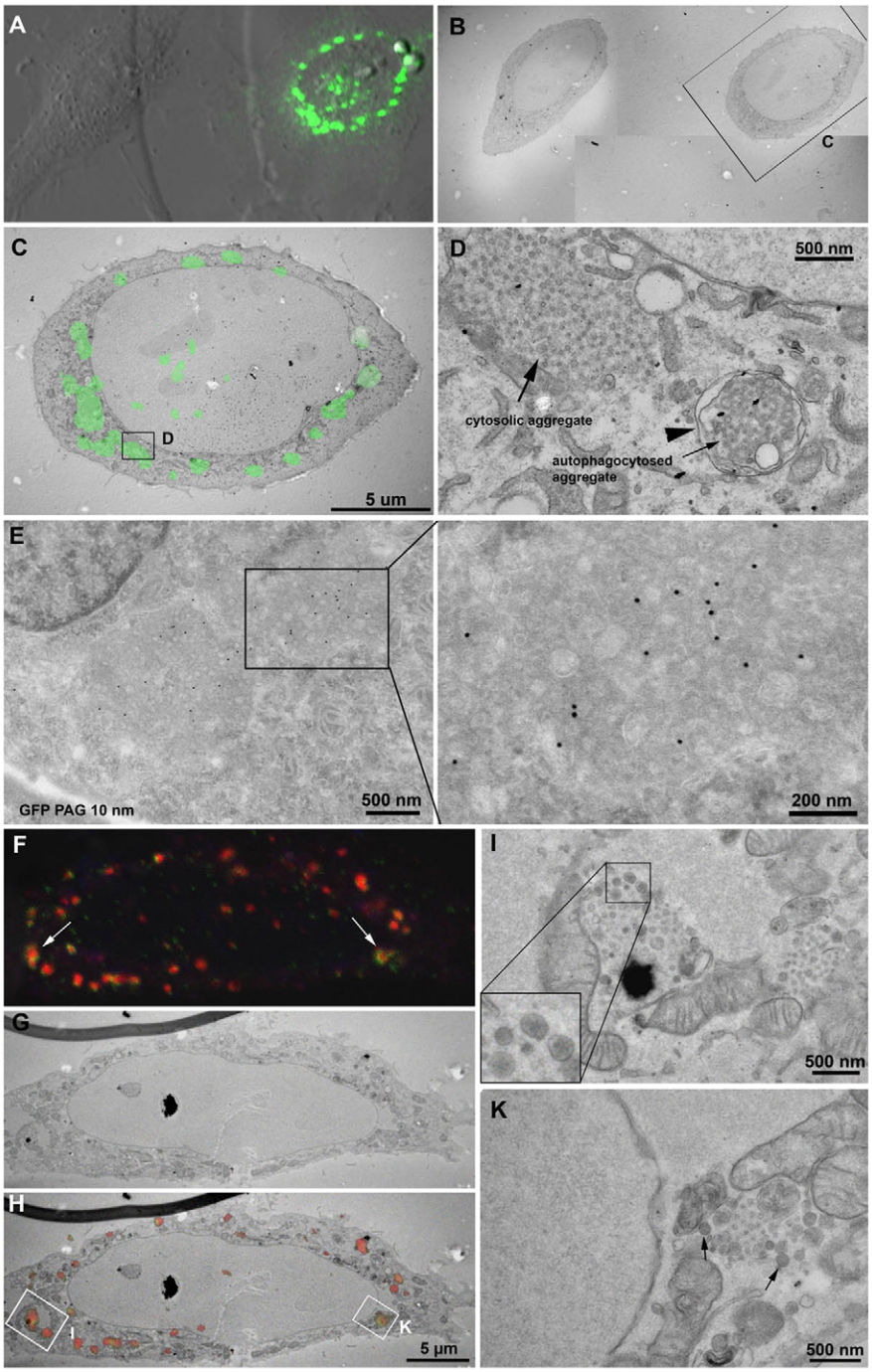

Fig. 3. Ultrastructural characterization of NBR1 aggregates by correlative light/electron microscopy. (**A**) HeLa cells were transfected with GFP-NBR1 for 24 hours and CLEM analysis was performed. (**B**) Spatial alignment of the electron micrograph with the confocal image. (**C**) Higher magnification image with direct overlay of the electron micrograph and the fluorescent image. (**D**) At higher magnification the GFP–NBR1-positive structures could be identified as aggregate-like structures (arrows in D), which were found either in a cytosolic, non-membrane-bound form or clearly sequestered within double-membrane-surrounded vesicles, resembling typical autophagosomes (arrowhead in D). (**E**) The GFP–NBR1 clusters were also apparent by immuno-EM using antibodies against GFP. The relationship between NBR1 aggregates and peroxisomes was further investigated in HeLa cells transfected with Cherry-NBR1 and the peroxisomal marker GFP–PMP34. (**F**) Confocal microscopy revealed very frequent colocalization of peroxisomes with Cherry–NBR1-positive structures (arrows in F). (**G**,**H**) Further CLEM analysis of the sample revealed similar cytosolic aggregates as in cells transfected with only GFP-NBR1. (**I**,**K**) At higher magnification we observed many peroxisome-like vesicles (enlarged in the inset in I, arrows in K), which often seemed to be localized at the periphery of the aggregates. Scale bars as indicated.

To further verify that exogenously expressing NBR1 leads to pexophagy we repeated these experiments in ATG5 knockout MEFs, an autophagy deficient cell line. To quantify changes in peroxisome numbers, we immunostained the MEFs for endogenous catalase and determined the peroxisome density (number of peroxisomes per cell volume). There was no significant change in peroxisome numbers in $Atg5^{-/-}$ MEFs when Cherry–NBR1 was exogenously expressed, whereas a significant loss of peroxisomes was observed in wild-type ($Atg5^{+/+}$) MEFs compared to non-transfected cells (Fig. 4C,D). These results were further verified by immunoblot analysis for changes in peroxisomal proteins. We found that both catalase and PMP70 levels decreased in the wild-type cells but not in the autophagy deficient cell line (Fig. 4E). Therefore, these results suggest that NBR1 can promote the activation of pexophagy. Interestingly, we found that there is no difference in the percentage of NBR1 clustered with peroxisomes between the two cell lines (Fig. 4F), yet there is a significant decrease in peroxisomes (Fig. 4E). These results may indicate that the clustering of NBR1 with peroxisomes precedes targeting to autophagosomes/lysosomes.

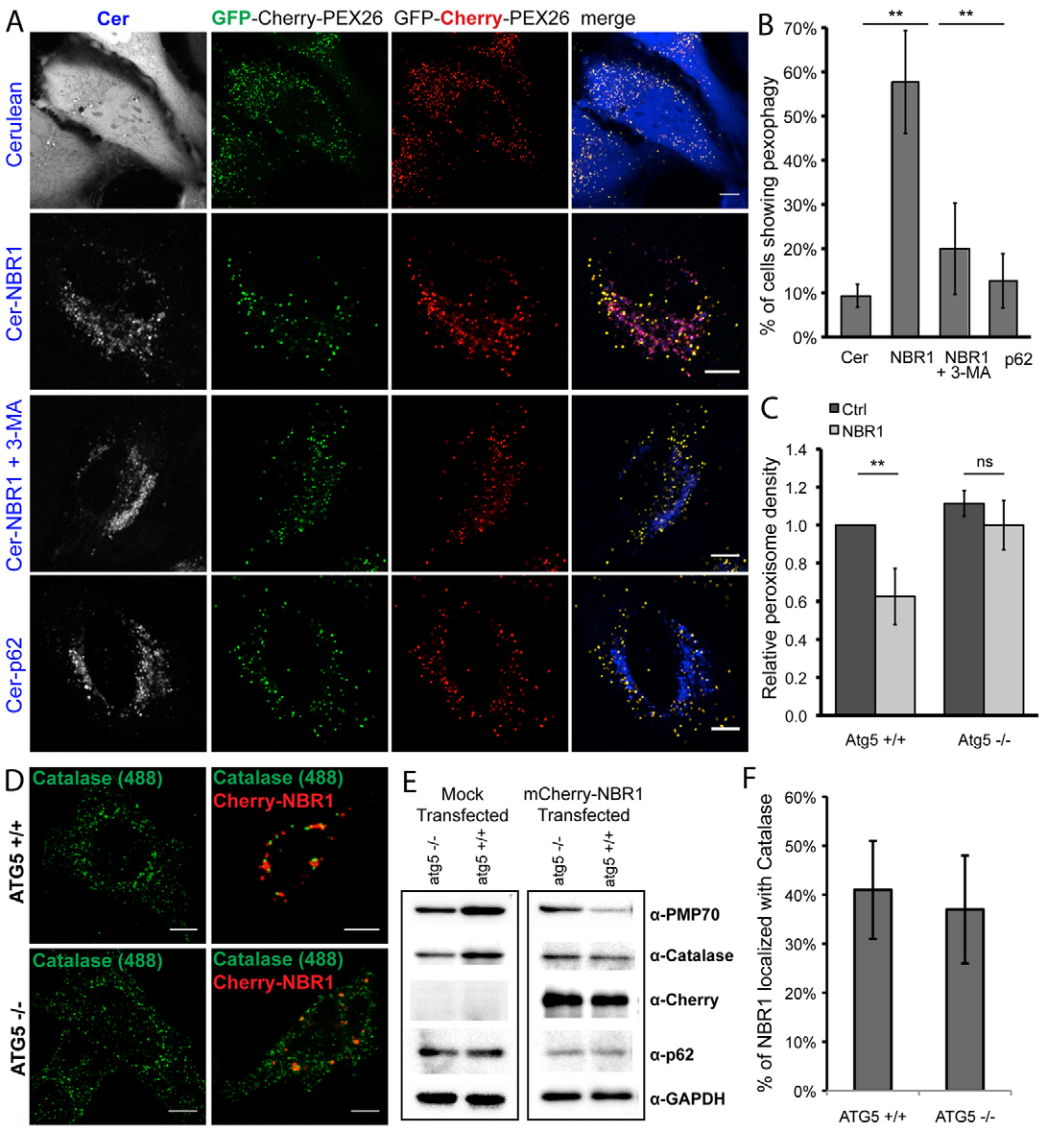

Fig. 4. Increased pexophagy in response to exogenous expression of NBR1. (**A**) Representative images of cells cotransfected with GFP-Cherry-PEX26$_{TM}$ and Cerulean (Cer), Cer-NBR1 or Cer-p62. Also shown is a representative cell treated with 3-MA. (**B**) Quantification of the percentage of cells in A that had increased pexophagy, using the RG-lysosome assay (see Materials and Methods for definition of increased pexophagy). (**C**) The number of catalase-positive punctate structures per cell volume of cells in D were quantified and normalized to their respective untransfected cells. (**D**) *Atg5*$^{+/+}$ and *Atg5*$^{-/-}$ MEFs were transfected with Cherry-NBR1 and immunostained for endogenous catalase. (**E**) Immunoblot analysis of *Atg5*$^{+/+}$ and *Atg5*$^{-/-}$ MEFs, either mock transfected or transfected with Cherry-NBR1. (**F**) A graph of the percentage of Cherry–NBR1 that colocalized with peroxisomes (catalase). The average of at least three independent experiments with standard deviations, determined from at least 50 cells from each experiment, is shown. ***P*=0.001–0.01, ns *P*>0.05. Scale bars: 10 µm.

NBR1 can promote pexophagy independently of p62

The activation of pexophagy by elevated NBR1 levels suggests that the amount of NBR1 in the cell may partly regulate pexophagy. The fact that NBR1 upregulated pexophagy at endogenous p62 levels suggests that p62 may not be strictly required for pexophagy during elevated NBR1 levels. Hence, we asked whether NBR1 could target peroxisomes to lysosomes independently of p62. To ascertain the requirement for p62 in NBR1-dependent pexophagy, we repeated the NBR1 RG-lysosome assay in cells where p62 expression was knocked down. In p62 siRNA-treated cells, Cer–NBR1-expressing cells still showed only a slight decrease in pexophagy compared to Cer–NBR1-expressing cells treated with non-targeting siRNA (Fig. 5A). However, these cells showed a significant increase in ‘red-only’ signal compared to control (Cer) or Cer–p62-expressing cells (Fig. 5A). Again there was no significant difference between cells expressing the siRNA resistant Cer–p62 and Cerulean alone, in both control siRNA and p62 knockdown conditions. These results suggest that NBR1 is sufficient to target peroxisomes to lysosomes for degradation in the absence of p62.

p62 increases the efficiency of NBR1-mediated pexophagy

The observations that p62 was not necessary in the presence of elevated NBR1 expression (Fig. 5A) but was required at endogenous NBR1 levels (Fig. 1) suggest that p62 may play a

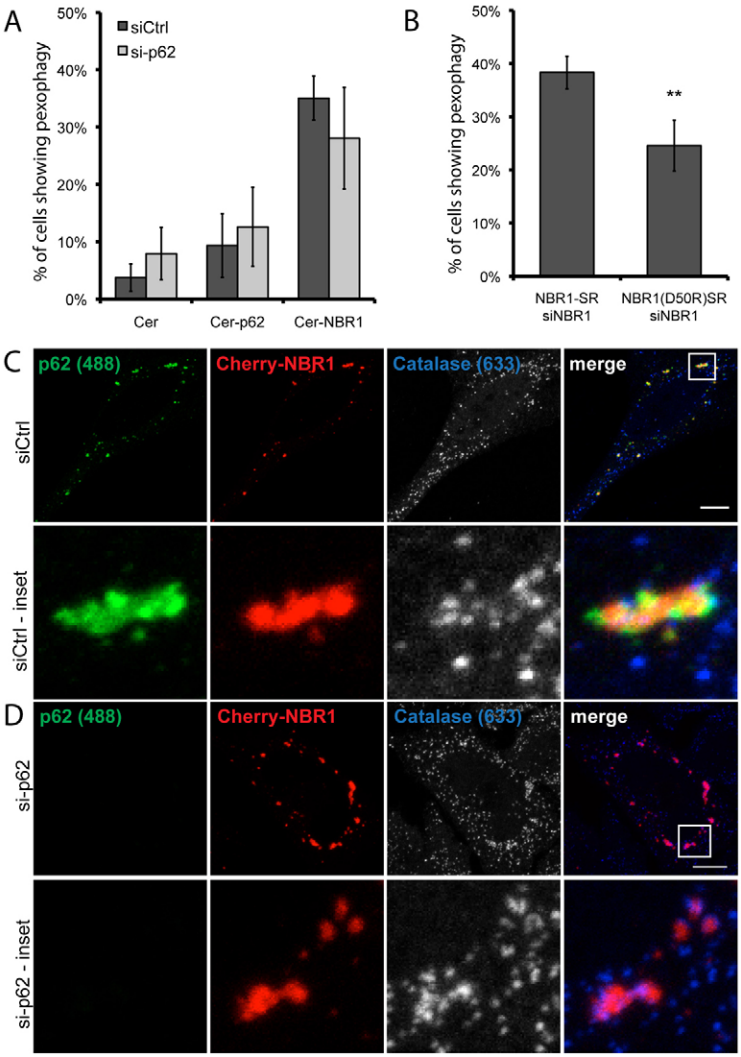

Fig. 5. NBR1 promotes pexophagy independently of p62, but p62 increases efficiency of NBR1-mediated pexophagy. (**A**) Bar graph of the percentage of cells showing increased pexophagy as determined by the RG-lysosome assay. Cells treated with either control siRNA or siRNA against p62 were transfected with Cer, Cer-NBR1, or siRNA-resistant Cer-p62 plasmids. The percentage of cells with increased pexophagy was determined by counting at least 50 cells. (**B**) Bar graph of the percentage of cells showing increased pexophagy in NBR1 knockdown cells expressing either siRNA resistant Cer–NBR1 or Cer–NBR1(D50R). For A and B the means ± s.d. were calculated from three independent experiments. $^{**}P=0.001$–0.01. (**C**) Cells expressing Cherry–NBR1were fixed and immunostained for endogenous catalase and p62. (**D**) p62-siRNA-treated cells were transfected with Cherry–NBR1 and immunostained for p62 and catalase as in C. The boxed regions in C and D are shown enlarged in the bottom row in each panel. Scale bars: 10 μm.

secondary role in the targeting of peroxisomes to lysosomes. To test this hypothesis, we compared the efficiency of pexophagy in cells expressing a mutant of NBR1, which is deficient in p62-binding (NBR1 D50R) to wild-type NBR1. NBR1 interacts with p62 via its PB1 domain and a single residue mutation within the PB1 domain (D50R) prevents this interaction (Kirkin et al., 2009a). To directly compare the D50R mutant with wild-type NBR1, siRNA-resistant (SR) versions of NBR1 constructs were expressed in cells where endogenous NBR1 was knocked down using siRNA. Under these conditions the NBR1 D50R mutant was less efficient in inducing pexophagy than wild-type NBR1 (Fig. 5B). The decrease in efficiency was not due to the instability of the mutant protein, since the expression of this and subsequently discussed mutant NBR1 proteins was checked by western blot analysis (supplementary material Fig. S5B).

To verify that p62 does interact with NBR1 during pexophagy, we examined the cellular localization of endogenous p62 in cells expressing Cherry–NBR1. We found that endogenous p62 colocalized with the NBR1/peroxisome clusters (Fig. 5C). Interestingly, close examination of these NBR1/p62/peroxisome clusters showed that p62 did not completely overlap with NBR1, but also formed punctate structures juxtaposed to the NBR1/peroxisome cluster structures (Fig. 5C).

Next we examined whether p62 was required for NBR1/peroxisome cluster formation. We found that even upon knocking down the endogenous p62, NBR1 was able to induce clustering of peroxisomes (Fig. 5D). Combined with the observation that elevated p62 expression alone did not cause peroxisome degradation (Fig. 4B; Fig. 5A), but was required for pexophagy at endogenous levels of NBR1 (Fig. 1), the above results suggest that p62 is not involved in the clustering and may not be required for NBR1 interaction with peroxisomes. Its role in pexophagy may be to increase the efficiency of NBR1-mediated targeting of peroxisomes to autophagosomes.

Homo-oligomerization of NBR1 is required for NBR1-dependent pexophagy

The homo-oligomerization of p62 is required for its targeting to nascent autophagosomes (Itakura and Mizushima, 2011). p62 homo-oligomerizes through the self-interaction of its PB1 domain (Lamark et al., 2003; Wilson et al., 2003). Although NBR1 also possesses a PB1 domain (through which it interacts with p62), it instead forms homo-oligomers via its coiled-coil domain (CC1) (Kirkin et al., 2009a). It is not known, however, whether self-oligomerization is required for targeting its cargo to autophagosomes. In order to address this question, we expressed

the NBR1 construct, NBR1 ΔCC1, where the coiled-coil domain was deleted. This construct is defective in homo-oligomerization (Kirkin et al., 2009a). Although this mutant can still cause peroxisome clustering, clustering was less efficient in the absence of endogenous wild-type NBR1 (Fig. 6A,B). Additionally, the RG-lysosome assay indicated that it targeted peroxisomes to lysosomes much less efficiently than wild-type NBR1 (Fig. 6C). In fact, there was no significant difference between NBR1 ΔCC1 compared to the control vector (Cer). Therefore, these results suggest that homo-oligomerization of NBR1 is required for efficient targeting of peroxisomes to autophagosomes.

LIR motifs of NBR1 are required for pexophagy

One characteristic of autophagy receptors is their ability to interface between the substrate and autophagosomes. The latter is accomplished by the LC3-interacting region (LIR), which is required for autophagy receptors to bind the autophagy factor LC3. It has been previously shown that NBR1 mediates targeting of polyubiquitylated aggregates to autophagosomes and that NBR1 contains two LIRs (LIR1 and LIR2) (Kirkin et al., 2009a). To determine whether the LIRs of NBR1 are required for pexophagy we constructed an NBR1 mutant where LIR1 is mutated and LIR2 deleted. This construct, called NBR1(LIR_{mut}), formed peroxisome clusters at similar levels as wild-type NBR1 (Fig. 6D). However, its pexophagy activity was significantly decreased compared to the wild-type NBR1 (Fig. 6E), suggesting that the LIR motifs are required for pexophagy and not for NBR1/peroxisome clustering.

The J and UBA domains of NBR1 are required for pexophagy

Previously we showed that an increase in ubiquitylated proteins on peroxisomes resulted in their targeting to autophagosomes for degradation (Kim et al., 2008). This suggests that the ubiquitin binding domain of NBR1, the UBA domain, may be required for binding to peroxisomes. Recently, the JUBA domain (hereafter for simplicity referred to as the J domain) – a novel, membrane-interacting, amphipathic α-helix region preceding the UBA domain – was found to be necessary for binding to endosomes (Mardakheh et al., 2010). Hence, we wanted to test if the J domain is also required for peroxisome binding.

First, we determined whether these domains were required for clustering of peroxisomes with NBR1. When both the J and UBA domains were deleted (GFP–NBR1 ΔJ-ΔUBA), clustering was

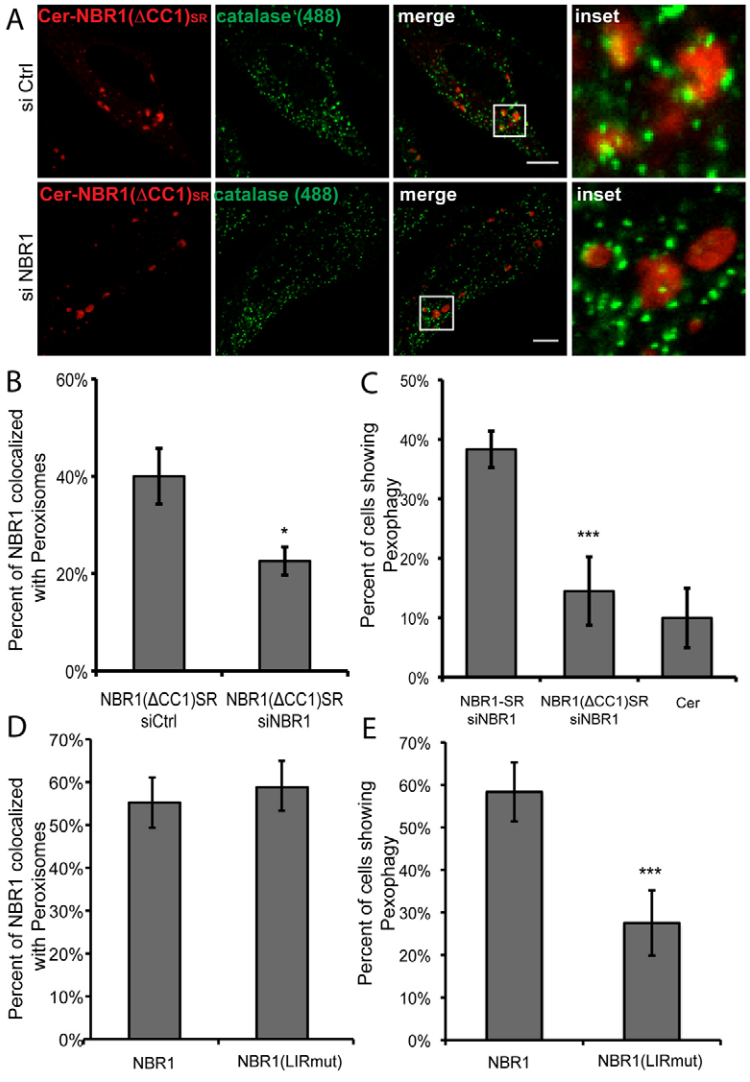

Fig. 6. Homo-oligomerization of NBR1 and LIR is required for pexophagy. (**A**) HeLa cells treated with either control siRNA or siRNA against NBR1 were transfected with an siRNA-resistant Cer-NBR1(ΔCC1) and immunostained for endogenous catalase. Shown are maximum projections of Z-stack images of 1.4 mm slices. Scale bars: 10 μm. (**B**) Quantification of percentage of cells showing colocalization of NBR1 with peroxisomes. Data are from three independent experiments ($n>50$). The percentage of NBR1 colocalized with catalase was determined using the Manders' M(Cherry) coefficient from a single confocal image. The two averages were significantly different ($P<0.01$). (**C**) RG-lysosome assay for pexophagy in NBR1 knockdown cells expressing either $NBR1_{SR}$, Cer–NBR1(ΔCC1)$_{SR}$ or Cerulean. The percentage shown is the average of three independent experiments ($n>50$). ***The Cer–NBR1(ΔCC1)$_{SR}$-expressing cells were significantly different from $NBR1_{SR}$ cells ($P<0.001$). (**D**) Quantification of colocalization of Cherry–NBR1 and Cherry–NBR1(LIR_{mut}) with peroxisomes as in B. (**E**) RG-lysosome assay for pexophagy for cells expressing either NBR1 or NBR1(LIR_{mut}). ***The Cer–NBR1(LIR_{mut})-expressing cells were significantly different from $NBR1_{SR}$ cells ($P<0.001$). Values are means ± s.d.

not observed (Fig. 7A,E). Similarly, deletion of the J domain (NBR1 ΔJ) also abrogated formation of peroxisome/NBR1 clusters (Fig. 7B,E). However, when only the UBA was deleted and the J domain retained (NBR1 ΔUBA), clustering occurred (Fig. 7C). The extent of clustering was quantified by calculating the percentage of NBR1 that colocalized with peroxisomes, using the Manders' colocalization coefficient. The colocalization of NBR1 ΔUBA with peroxisomes was similar to that of wild-type NBR1 (Fig. 7E).

Interestingly, the NBR1 ΔUBA mutant localized to both punctate and tubular structures that resembled mitochondria (Fig. 7C). Upon further investigation, this mutant was indeed found to colocalize with the mitochondrial marker mito-RFP in HeLa cells (Fig. 7D) and COS7 cells (data not shown). However, NBR1, NBR1 ΔJ and NBR1 ΔJ-ΔUBA were not found to colocalize with mitochondria (data not shown). We also examined the colocalization of the NBR1 ΔUBA mutant with other organelles. A comparison of colocalization coefficients of NBR1 ΔUBA versus the wild-type NBR1 show that there is increased colocalization of NBR1 ΔUBA with the ER, lysosomes, the Golgi apparatus and mitochondria (supplementary material Fig. S6). p62 does not have any domain homologous to the J domain. When we fused the J domain to p62 with its own UBA domain deleted, we also found that p62-J_N-ΔUBA_N localized to mitochondria (supplementary material Fig. S7D–F). The wild-type p62 or another variant where the J domain is located N-terminal to the UBA domain of p62 does not localize to mitochondria (supplementary material Fig. S7A–C). Therefore, these observations suggest that the J domain is capable of binding membrane bilayers other than peroxisomes in the absence of the UBA domain. Hence, the UBA domain may play a regulatory role in the targeting of NBR1 to specific membranes.

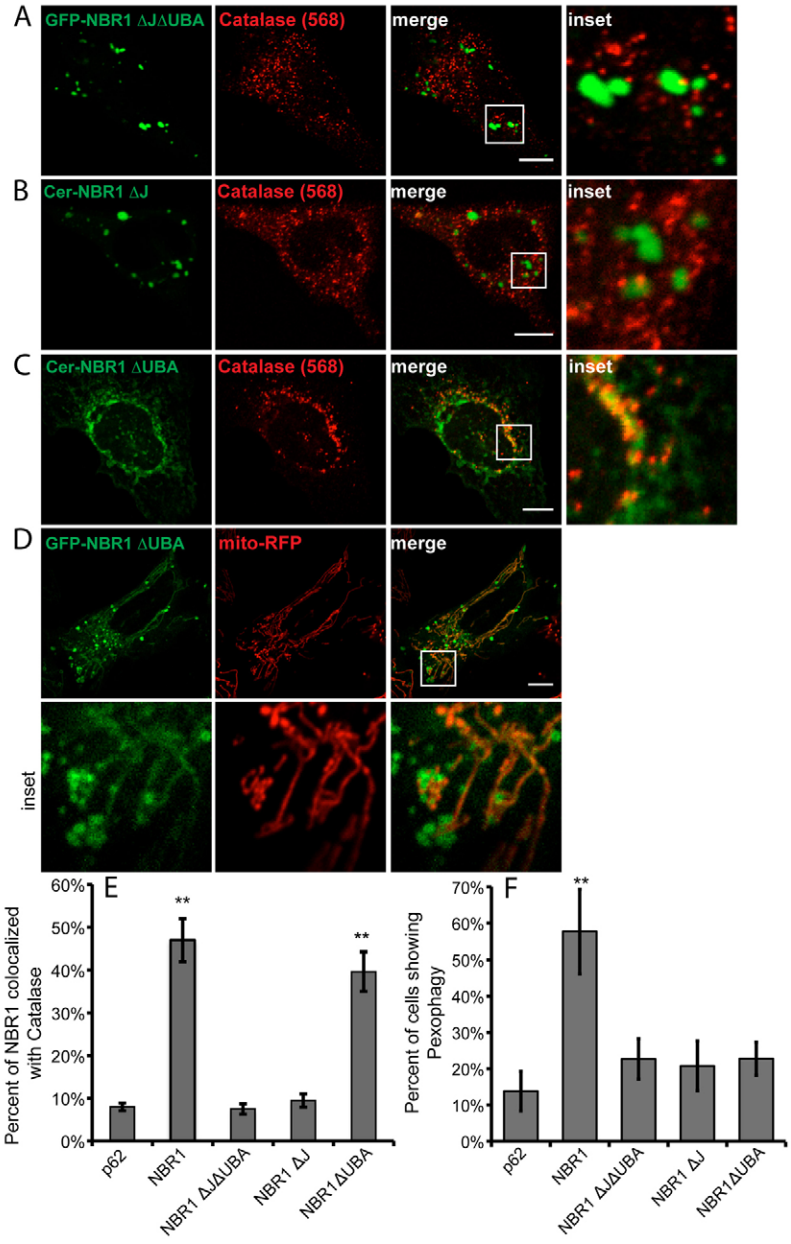

Fig. 7. Both the J domain and the UBA domain of NBR1 are required to induce pexophagy. HeLa cells were transfected with plasmids encoding (**A**) GFP–NBR1 ΔJΔUBA; (**B**) Cer–NBR1 ΔJ; or (**C**) Cer–NBR1 ΔUBA. The cells were fixed and immunostained for endogenous catalase. The boxed area is enlarged in the images labeled 'inset'. (**D**) GFP–NBR1 ΔUBA-expressing cells were cotransfected with mito-RFP. The boxed area is enlarged in the images below. (**E**) Colocalization of Cherry-tagged NBR1 or p62 with endogenous catalase. Manders' thresholded colocalization coefficients were determined for at least 50 cells for each condition. Error bars represent standard error of the mean; $^{**}P<0.01$. Averages of three independent experiments are shown. (**F**) Quantification of the RG-lysosome assay for pexophagy in cells expressing the autophagy receptor proteins and mutants as indicated. HeLa cells were transfected with plasmids expressing both the autophagy receptor and GFP–Cherry–PEX26 and live-cell images were acquired. The averages from at least three independent experiments are shown. At least 50 cells were quantified for each set of experiments. $^{**}P<0.001$ compared to p62. Scale bars: 10 μm.

To determine whether the various NBR1 deletion mutants can promote pexophagy, we coexpressed them with GFP–Cherry–PEX26$_{TM}$ and subjected them to the RG-lysosome assay. The three mutants NBR1 ΔUBA, NBR1 ΔJ and NBR1 ΔJ-ΔUBA did not show any significant increase in pexophagy compared to control (Fig. 7F). Only the wild-type NBR1, containing both the J and UBA domains, resulted in a significant increase in pexophagy. Therefore, these results show that although the J domain is required for peroxisome binding, both the J domain and UBA domains are required for targeting peroxisomes to autophagosomes for lysosomal degradation.

The J domain of NBR1 enables p62 to mediate pexophagy

To further test the role of the UBA and J domains in pexophagy, we examined whether they can confer pexophagy activity on p62. p62 has similar domain architecture to NBR1; it contains all the domains required to induce pexophagy, except for the amphipathic J domain preceding the UBA domain (Fig. 8A). Like NBR1, p62 forms homo-oligomers, possesses a UBA domain and possesses an LIR domain. Yet p62 cannot induce pexophagy upon overexpression in cells (Fig. 4B). Therefore, we asked whether the J-domain of NBR1 confers its specificity for peroxisomes. To test this hypothesis, we constructed a number of domain-swap mutants of p62 where its UBA domain was replaced with the J and/or UBA domains of NBR1 (Fig. 8A). We also inserted the J domain of NBR1 immediately upstream of the UBA domain in p62 (p62-J$_N$-UBA$_p$). All chimeras containing the J domain exhibited clustering with peroxisomes (Fig. 8B), but when they were subjected to the RG-lysosome assay, only the p62 chimeras containing both the J domain and a UBA domain (of either NBR1 or p62) were able to cause an increase in pexophagy (Fig. 8C; supplementary material Fig. S8). Notably, the UBA domains of NBR1 and p62 were interchangeable and both promoted pexophagy, provided that the J domain was also present. The constructs containing only the J domain or UBA domain of NBR1 did not induce pexophagy above the level found for wild-type p62 and Cer control. Together with the analysis of NBR1 mutants these data suggest that both the J and UBA domains are required to promote selective degradation of peroxisomes.

Inhibiting PEX5 recruitment to peroxisomes prevents pexophagy

Next we asked how NBR1 might be recruited to peroxisomes. The importance of the UBA domain for selective binding of NBR1 to peroxisomes suggests that NBR1 is likely binding to a ubiquitylated protein on peroxisomes. One possible candidate is PEX5, a cytosolic receptor for peroxisomal matrix proteins. Peroxisome matrix proteins are imported into peroxisomes by the formation of a transient pore that consists of at least two proteins, PEX14 and PEX5. PEX14 is the membrane receptor that recruits the matrix protein receptor PEX5 to the peroxisomal membrane, and together they form a transient pore (Meinecke et al., 2010). It is thought that this transient pore is disassembled by ubiquitylation of PEX5 (Platta et al., 2007). We wanted to test if NBR1 is recruited to peroxisomes upon binding to ubiquitylated PEX5. To test this hypothesis we prevented PEX5 recruitment to peroxisomes by knocking down the expression of PEX14. Using quantitative PCR we confirmed that there was a 74% decrease in PEX14 mRNA upon treating HeLa cells with siRNA against PEX14 (Fig. 8D). Furthermore we observed that knocking down PEX14 disrupted the import of

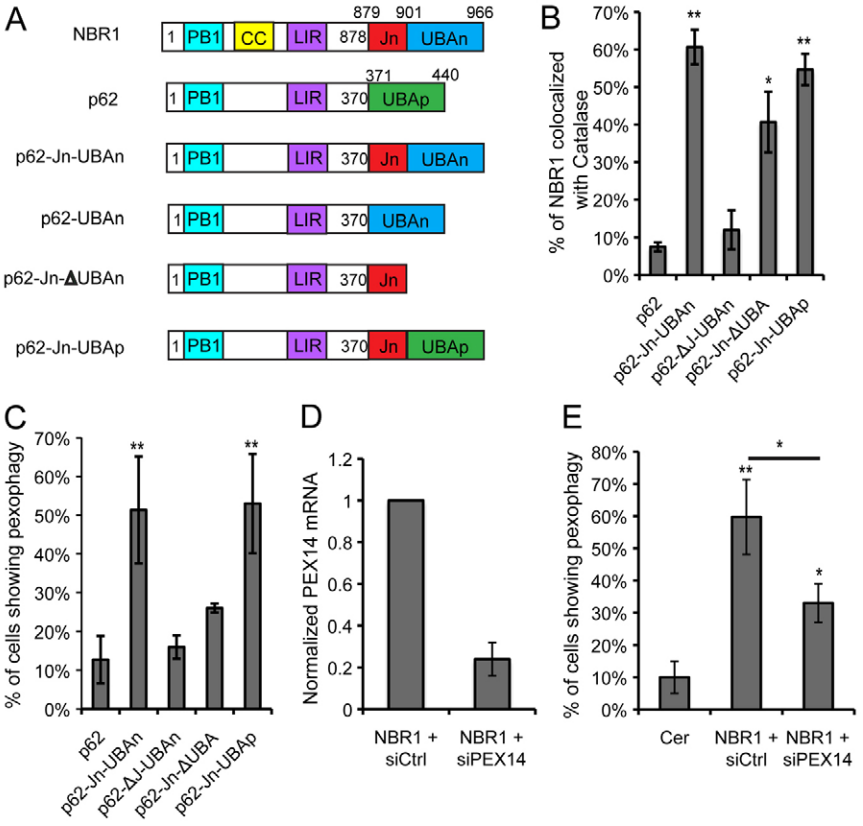

Fig. 8. The J domain of NBR1 is sufficient to confer peroxisome specificity on p62 and PEX14 knockdown decreases NBR1-induced pexophagy. (**A**) Schematic diagram of NBR1 and p62 domain mutants. CC, coiled coil domain; LIR, LC3-interacting domain. (**B**,**C**) Quantification of clustering (B) and the RG-lysosome assay (C) of HeLa cells transfected with Cerulean or Cerulean-tagged autophagy receptor proteins and mutants, as indicated. The means ± s.d. from three independent experiments are shown. At least 50 cells were quantified for each set of experiments, $n=3$. *$P<0.001$ compared to Cerulean-expressing cells. (**D**) Quantitative PCR of PEX14 mRNA levels in HeLa cells treated with control siRNA and PEX14 siRNA. (**E**) Quantification of pexophagy by the RG-lysosome assay in HeLa cells with PEX14 knockdown and NBR1 overexpression. HeLa cells were transfected with siRNAs and Cerulean-NBR1, as indicated, and GFP–Cherry–PEX26, and live cell images were acquired. The means ± s.d. from at least three independent experiments are shown. At least 50 cells were quantified for each set of experiments. *$P<0.01$; **$P<0.001$.

a PEX5 cargo, catalase, into peroxisomes, (supplementary material Fig. S9A, punctate versus cytosolic), suggesting that PEX14 knockdown prevents PEX5 recruitment to peroxisomes.

To determine whether NBR1 required ubiquitylated PEX5 to target to peroxisomes, we exogenously expressed Cherry–NBR1 in PEX14 siRNA knockdown cells. While Cherry–NBR1 clustered with PMP70-positive structures in PEX14-containing cells, in PEX14 depleted cells we found that Cherry–NBR1 did not colocalize with PMP70 positive structures, suggesting that it did not bind to peroxisomes (supplementary material Fig. S9B–E). When we examined these cells for changes in pexophagy upon NBR1 expression, we found that there was a significant decrease in pexophagy compared to control siRNA-treated cells. Yet, pexophagy was still higher than control (Fig. 8E). This may be the result of the incomplete knockdown of PEX14 (Fig. 8D; supplementary material Fig. S9), or it is equally likely that NBR1 is also binding to another ubiquitylated peroxisomal membrane protein. Nevertheless, these experiments suggest that the ubiquitylated PEX5 may be one component that recruits NBR1 to peroxisomes.

Discussion

Peroxisome numbers are highly regulated. Pexophagy rapidly removes superfluous or damaged peroxisomes (Till et al., 2012). Peroxisomes are also turned over in response to various cellular signals, such as starvation conditions. During amino acid deprivation peroxisomes are believed to be selectively degraded while mitochondria are protected from autophagic degradation (Gomes et al., 2011; Hara-Kuge and Fujiki, 2008; Rambold et al., 2011). The ubiquitin binding autophagy receptors are involved in selective targeting of organelles to autophagosomes for degradation. Here we demonstrate that substrate selectivity may be partly conferred by the autophagy receptors themselves. Using peroxisomes as substrates for selective autophagy we showed that NBR1, and not p62, is necessary and sufficient for the turnover of endogenous peroxisomes.

We report that the J and UBA domains of NBR1 are required for its specificity for peroxisomes. These domains confer specificity by mediating the selective binding of NBR1 to peroxisomes. An essential role for the J domain is supported by the observation that mutants lacking the J domain (NBR1 ΔJ and NBR1 ΔJΔUBA) did not colocalize with peroxisomes (Fig. 7). However, based on our results we hypothesize that the UBA domain is required for the specific recruitment of NBR1 to the peroxisomal membrane. NBR1 without the UBA domain (NBR1 ΔUBA) formed peroxisome/NBR1 clusters, but also exhibited increased colocalization with other organelle markers, such as the mitochondria, which was not observed with full length NBR1 (supplementary material Fig. S6). Similar non-selective binding to various bilayers via the J domain was also observed with the p62-J_N-ΔUBA construct, where the UBA domain of p62 was replaced with the J domain of NBR1 (Fig. 8; supplementary material Fig. S7). Adding a UBA domain from either p62 or NBR1 to the J domain (p62-J_N-$UBA_{P/N}$) prevented the nonspecific binding to mitochondria (supplementary material Fig. S7). These results suggest that the UBA domain may act as a regulator of NBR1 binding to peroxisomes, since the J domain in the absence of the UBA domain appears to bind non-specifically to any lipid bilayer.

There is a precedent for this type of membrane binding mechanism. A number of PI3P binding proteins, such as EEA1 and Vps27, target and bind to PI3P rich membranes via a two-step binding mechanism (reviewed in Kutateladze, 2006). Both EEA1 and Vps27 possess the PI3P binding domain, FYVE, and a membrane interaction loop (MIL). These proteins are initially targeted to a specific membrane by interaction of the FYVE domain with PI3P, resulting in a conformational change exposing the membrane interaction loop domain to insert into the lipid bilayer to anchor the protein to the target organelle. In fact, phosphoinositide-binding proteins are known to act as detectors of coincident localization signals to allow localization to specific membranes and membrane domains (reviewed in Carlton and Cullen, 2005). So, NBR1 may act as a coincidence detector requiring both the coincident biding of the UBA domain and the J domain to peroxisomes to effectively target peroxisomes for autophagic degradation. We favor this mechanism as it explains the non-specific binding of the UBA deletion mutant (NBR1 ΔUBA) and the inability of the J domain deletion mutant (NBR1 ΔJ) to bind to peroxisomes.

Interestingly, although NBR1 ΔUBA was able to bind peroxisomes, it was not able to increase the pexophagy levels. Instead, an increase in pexophagy required both the J and UBA domains. The inability of the J domain alone to induce pexophagy may in part be explained by the fact that it binds to more different organelles (substrates) than the wild type, which appears to bind mainly to peroxisomes. The non-selective binding of this mutant to a number of subcellular membranes may result in an increase in autophagy substrates, causing an effective decrease in peroxisome degradation.

The need for a UBA domain on NBR1 to induce pexophagy further supports our previous report showing that increasing ubiquitin moieties on the cytosolic face of peroxisomes induced pexophagy (Kim et al., 2008). However, the question remains as to which peroxisomal protein(s) is ubiquitylated to induce pexophagy. Here we demonstrate that one possible peroxisomal protein target is PEX5, a component of the peroxisomal transient pore complex that is required for the import of peroxisomal matrix proteins. PEX5 is likely the most frequently ubiquitylated protein on the peroxisomal membrane, as it must be removed to disassemble the transient pore and be recycled back to the cytosol to import other peroxisomal matrix proteins (Platta et al., 2007; Meinecke et al., 2010). We postulate that the overexpression of NBR1 increases the rate of NBR1 interaction with the ubiquitylated PEX5. This stabilizes the J-domain-mediated binding of NBR1 to the bilayer, resulting in the accumulation of NBR1 on the peroxisomal membrane. Pexophagy is likely induced when there is sufficient accumulation of NBR1 on peroxisomes. In other words, in order to target peroxisomes to autophagosomes, a ‘critical mass,’ or number of autophagy receptors on peroxisomes is likely required to target these organelles to nascent autophagosomes.

We found that knocking down p62 expression results in an increase in peroxisome numbers, but not to the same levels as observed for NBR1 or ATG12 knockdown (Fig. 1). Although we find that p62 is not required for pexophagy in an NBR1 overexpression system, it does increase efficiency. Thus, based on our critical mass hypothesis, NBR1 on peroxisomes likely recruits p62 in order to increase the number of autophagy receptors on the peroxisome surface and achieve the ‘critical mass’ required for efficient pexophagy. This is further supported by the observation that although both NBR1 and p62 can form independent punctate structures (Kirkin et al., 2009a), they

colocalize with each other on the substrate (Fig. 6C). Interestingly, the colocalization of p62 with NBR1 was only partial as there were distinct NBR1 and p62 structures juxtaposed to each other around peroxisomes. These structures may be analogous to the microdomains formed by the autophagy receptors p62 and NDP52 around *Salmonella* inside autophagosomes (Cemma et al., 2011; Mostowy et al., 2011; Zheng et al., 2009). However, the nature of these microdomains is not known.

Our finding that NBR1 is a receptor for pexophagy in mammalian cells suggests a mechanistic difference between the yeast and mammalian systems. Recently, Atg30 has been described to be the autophagy receptor for peroxisome turnover in *Pichia pastoris* (Farré et al., 2008). This protein is found localized on the peroxisomal membrane via its interaction with two peroxisomal membrane proteins, Pex14p and Pex3p. Unlike mammalian autophagy receptors it does not directly interact with Atg8, the yeast LC3 homologue, but instead interacts with Atg11 and Atg17 in order to target peroxisomes to autophagosomes. This interaction with the Atg11–Atg17 complex requires the phosphorylation of Atg30. Furthermore, Atg30 does not have an obvious ubiquitin binding domain, suggesting that its targeting to peroxisomes is not ubiquitin dependent. However, a pexophagy receptor, Atg36, that binds to Pex3 on peroxisomes and to Atg8 and the adaptor Atg11 was recently discovered in *Saccharomyces cerevisiae* (Motley et al., 2012). Apart from the lack of ubiquitin in the targeting role, this is more similar to the situation with NBR1 in mammalian pexophagy described here.

Materials and Methods

Plasmids

Cherry-NBR1, GFP-NBR1(ΔCC1), Cherry-NBR1(D50R), Cherry-p62, Lamp1-GFP, Lamp1-Cer, ss-GFP-KDEL, mito-RFP, mito-GFP, GFP-LC3 and PMP34-GFP were described previously (Kim et al., 2008; Kirkin et al., 2009a; Mitra et al., 2009). All other plasmids were constructed using standard protocols or Gateway recombination cloning, and were sequenced for confirmation (The Centre for Applied Genomics, Toronto, ON, Canada, and Sequencing Core Facility, University of Tromsø, Norway). Primers were produced by Sigma Genosys (Oakville, ON, Canada) and Invitrogen. Cloning strategies and primer sequences used are available upon request.

The GFP-NBR1(ΔJΔUBA) construct contains the first 875 codons of the NBR1 gene, while GFP-NBR1(JΔUBA) has the first 919 codons of NBR1 within Clontech pEGFP-C1. NBR1(D50R)(ΔJ) group of plasmids were constructed from NBR1(D50R) plasmid but the base pairs pertaining to residues 877–902 were deleted. For simplicity, these constructs, although D50R mutants, are referred to as NBR1(ΔJ) in the text and figures. SiRNA-resistant (SR) alleles of wild-type NBR1 and the NBR1(ΔCC1) and NBR1(D50R) mutants were constructed by introducing a silent mutation at L839 by site-directed mutagenesis. A schematic representation of the constructs of Cer-p62-$J_N$$UBA_N$, p62-$UBA_N$, p62-$J_N$-ΔUBA and p62-$J_N$-$UBA_p$ are shown in Fig. 8A.

GFP-Cherry-$PEX26_{TM}$ was constructed in several steps. First, the PEX26 ORF from pSPORT-PEX26 (Invitrogen) was cloned into the *Eco*RI and *Sal*I sites of pEGFP-C1, and then it was truncated by PCR. Finally, the mCherry gene was inserted into the *Bgl*II and *Bam*HI sites of the vector to generate GFP-Cherry-$PEX26_{TM}$.

Reagents and antibodies

Leupeptin (Bioshop, or Enzo Life Sciences) was used at 0.5 mM and E-64 (Enzo Life Sciences) at 2 μM. 3-methyladenine (3-MA; Sigma-Aldrich) was dissolved directly in media at 10 mM. siRNA targeting NBR1 (5′-GGAGUGGAUUUA-CCAGUUAUU-3′), p62 (5′-GCAUUGAAGUUGAUAUCGAUTT-3′), ATG12 (5′-GUGGGCAGUAGAGCGAACATT-3′), and non-targeting controls (5′-UU-CUCCGAACGUGUCACGUTT-3′ or 5′-UAAGGCUAUGAAGAGAUACTT-3′) were produced by GenePharma (Shanghai, China). The NDP52 siRNA (5′-UUCAGUUGAAGCAGCUCUGUCUCCC-3′) and the rabbit polyclonal anti-NDP52 was a gift from Dr John Brumell.

Primary antibodies used in this study were rabbit polyclonal anti-catalase (EMD Biosciences, Calbiochem, Darmstadt, Germany), mouse monoclonal anti-p62 (BD Biosciences), rabbit polyclonal anti-NBR1 (Kirkin et al., 2009a), mouse monoclonal anti-NBR1 (Abnova, Taipei City, Taiwan), rabbit polyclonal anti-GFP (T. Johansen) and mouse anti-actin (Sigma-Aldrich). All fluorescent anti-mouse and anti-rabbit Alexa Fluor 488, 568 and 633 secondary antibodies were from Invitrogen. HRP-conjugated goat anti-mouse IgG and goat anti-rabbit IgG secondary antibodies were from Cedarlane. 10 nm Protein A gold (CMC, Utrecht, The Netherlands).

Cell culture

HeLa and MEF cells were grown in DMEM supplemented with 10% fetal bovine serum (FBS; Invitrogen). For live-cell imaging, cells were grown, manipulated and imaged in LabTek chamber slides (Nalgene Nunc, Rochester, NY). For immunofluorescence, cells were grown either in LabTek chamber slides or on no. 1 glass coverslips. Plasmids were transfected using Fugene-HD (Roche) or Lipofectamine-2000 (Invitrogen) or TransIT LT1 (Mirus Bio). siRNAs were transfected using Lipofectamine-2000 according to the manufacturer's instructions. For simultaneous siRNA knockdown and plasmid overexpression, siRNA alone was transfected on the first day, and siRNA and plasmids were transfected simultaneously on the second day, using Lipofectamine-2000. For the RG-lysosome assay, cells were treated with leupeptin and E-64 beginning on the day after plasmid transfection, to prevent degradation of protein inside lysosomes and allow detection of Cherry signal. When specified, cells were treated with 3-MA, beginning on the day after plasmid transfection. Cells were imaged 2 and/or 3 days after plasmid transfection. Prior to live imaging, the medium was changed to CO_2-independent medium (Invitrogen) containing 10% FBS, and leupeptin, E-64, and 3-MA, as needed.

Microscopy

Laser-scanning confocal microscopy was performed on a Zeiss LSM710 with a 63×/1.4 Plan-Apochromat oil objective or on a Leica TCS SP5 with a 63×/1.2 NA water immersion objective. When required, images were acquired in Z-sections of 0.5 to 1.0 μM thickness. Live cell imaging was performed at 37℃ in CO_2-independent medium containing 10% FBS, and leupeptin, E-64 and 3-MA, as specified. For immunofluorescence, cells were fixed using 3.7% paraformaldehyde (Electron Microscopy Sciences) in PBS for 15 minutes and permeabilized using 0.1% Triton X-100 (Fisher Scientific) in PBS for 15 minutes, followed by incubation with the appropriate primary and secondary antibodies for 2 hours (or overnight at 4℃), and 1 hour, respectively. For all NBR1/peroxisome clustering experiments, the same pre-set microscopy acquisition setting was always used (laser power, master gain, etc.) to ensure that images from experiments performed on different days could be directly compared.

Correlative light and electron microscopy

Correlative light and electron microscopy (CLEM) was performed on HeLa cells grown on gridded coverslips (EMS, Hatfield, PA, USA) and transfected with GFP-NBR1 alone or double transfected with GFP-PMP34 and Cherry-NBR1 for 24 hours as described earlier. Cells were fixed in 4% formaldehyde, 0.2% glutaraldehyde in 0.1 M phosphate buffer, pH 7.2, embedded in Moviol and observed on a confocal microscope (LSM 710, Carl Zeiss MicroImaging, Inc.) with 63× or 20× objectives, using the appropriate channels and differential interference contrast (DIC) microscopy. We used maximum projections from Z-stacks (seven slices, 4–6 μm total height) taken at 63× magnification for the final overlay images. The localization of cells of interest on the gridded coverslip was recorded using DIC microscopy. After detaching the coverslips in phosphate buffer (1–2 hours at room temperature) they were fixed in 2% glutaraldehyde, followed by 2% OsO_4 and 1.5% KFeCN in the same buffer. Coverslips were then stained en bloc with 4% uranyl acetate for 1 hour, dehydrated in graded ethanol series and embedded with Epon filled gelatin capsules placed on top of the coverslip. The coverslips were removed after polymerization with 48% hydrofluoric acid (Merck, Germany) and the blocks were then trimmed down to the regions previously identified on the confocal microscope and now imprinted on the Epon block. Sections of 150–200 nm thickness were then cut parallel to the substratum on a Leica Ultracut and post-stained with lead citrate (2 minutes, Fig. 8B–D) or not stained (Fig. 8F–I). Electron micrographs were taken at indicated magnifications and overlaid with the confocal images using Adobe Photoshop. Importantly, we would like to point out that the confocal images represent total fluorescence from the whole cell volume, whereas electron micrographs only represent 150–200 nm thick sections, thereby explaining the fluorescent signals outside apparent cell borders and above the nuclei. Cells for immuno-EM were prepared as described previously (Bjørkøy et al., 2005) and immunolabeled with antibodies against GFP followed by 10 nm Protein A gold.

Image analysis

Images were analyzed using Volocity software (Perkin Elmer). For quantification of peroxisome intensity by catalase staining, all conditions were treated simultaneously using the same antibody conditions. All mean intensity was normalized against the control siRNA performed on the same day. Furthermore, to capture the mean intensity from the catalase staining within the whole cell, images were acquired with an open pinhole. At least 100 cells were quantified, normalized against the control and averaged per experiment. For quantification of peroxisome

density in MEFs, the number of catalase-stained structures was divided by the volume of each cell, and the averages were normalized to the $Atg5^{+/+}$ untransfected controls. At least 50 cells were analyzed for each condition.

For quantification of the RG-lysosome assay, all images were acquired using settings calibrated such that the GFP and mCherry fluorescence intensities ($I_{G/R}$) were approximately equal (i.e. $I_{GFP}/I_{mCherry}=1$). We found that this acquisition setting gave equivalent readings even on different days. Therefore a preset acquisition setting was used for all RG-lysosome assays. A cell was considered to be undergoing increased pexophagy if the number of 'red-only' pixels were greater than 20% of the total 'red' pixels. To calculate the red-only pixels, all the pixels with Cherry signal above a predetermined threshold were first determined, and both the GFP (green) and Cherry (red) signals were collected for each of these pixels. A pixel was considered red-only if the Cherry fluorescent signal was at least three times higher than the GFP fluorescent signal. A cell was considered to have an increase in pexophagy if at least 20% of the Cherry containing pixels were red-only (supplementary material Fig. 4). The percentage of cells with 20% or more red-only pixels was reported.

Manders' thresholded colocalization coefficients were determined for at least 50 cells for each condition using ImageJ (NIH, Bethesda) and the JaCoP plugin (Bolte and Cordelières, 2006). Cells above a pre-determined expression level, as determined by the fluorescence signal from NBR1 expression levels, were used. The threshold was set to exclude structures not corresponding to NBR1/p62 puncta or peroxisomes. The percentages reported correspond to the amount of mCherry–positive pixels that are also catalase-positive. Error bars represent standard error of the mean. For statistical significance a two-tailed *t*-test was performed using Microsoft Excel 2010.

Western blots

Cells were lysed with 100 mM Tris pH 9 containing 1% SDS (Bio-Rad) and Halt protease inhibitor cocktail (Thermo Scientific), and the lysate was heated at 100℃ with vortexing for 20 minutes, then centrifuged at 13,000 ***g*** for 20 minutes. The protein concentration in the supernatant was determined by BCA assay (EMD Novagen), equivalent sample amounts were subjected to SDS-PAGE, and protein was transferred to 0.45 µm BioTrace PVDF membrane (Pall) and probed with the appropriate primary and HRP-conjugated secondary antibodies following standard protocols. Blots were developed using Luminata Crescendo (Millipore), ECL Plus or ECL Advance reagents (GE Healthcare) and detected on blue film (AGFA) or Hyperfilm (GE Healthcare).

Acknowledgements

We are indebted to Dr John Brumell for reagents and helpful discussion pertaining to the project and the BioImaging core facility at the Institute of Medical Biology, University of Tromsø for the use of instrumentation and expert assistance.

Funding

This work was funded by an operating grant from the Canadian Institutes of Health Research [grant number MOP-111164 to P.K.K.]; an infrastructure grant from Canada Foundation for Innovation [grant number 23584 to P.K.K.]; the Ontario Research Fund [grant number 23584 to P.K.K.]; the Functional Genomics and the Biology and Biomedicine (FRIBIO) programs of the Norwegian Research Council [grant number 196898 to T.J.]; and the Norwegian Cancer Society [grant number 71043-PR-2006-0320 to T.J.].

Supplementary material available online at
http://jcs.biologists.org/lookup/suppl/doi:10.1242/jcs.114819/-/DC1

References

Bjørkøy, G., Lamark, T., Brech, A., Outzen, H., Perander, M., Overvatn, A., Stenmark, H. and Johansen, T. (2005). p62/SQSTM1 forms protein aggregates degraded by autophagy and has a protective effect on huntingtin-induced cell death. *J. Cell Biol.* **171**, 603-614.

Bolte, S. and Cordelières, F. P. (2006). A guided tour into subcellular colocalization analysis in light microscopy. *J. Microsc.* **224**, 213-232.

Carlton, J. G. and Cullen, P. J. (2005). Coincidence detection in phosphoinositide signaling. *Trends Cell Biol.* **15**, 540-547.

Cemma, M., Kim, P. K. and Brumell, J. H. (2011). The ubiquitin-binding adaptor proteins p62/SQSTM1 and NDP52 are recruited independently to bacteria-associated microdomains to target Salmonella to the autophagy pathway. *Autophagy* **7**, 341-345.

Ding, W. X., Ni, H. M., Li, M., Liao, Y., Chen, X., Stolz, D. B., Dorn, G. W., 2nd and Yin, X. M. (2010). Nix is critical to two distinct phases of mitophagy, reactive oxygen species-mediated autophagy induction and Parkin-ubiquitin-p62-mediated mitochondrial priming. *J. Biol. Chem.* **285**, 27879-27890.

Farré, J. C., Manjithaya, R., Mathewson, R. D. and Subramani, S. (2008). PpAtg30 tags peroxisomes for turnover by selective autophagy. *Dev. Cell* **14**, 365-376.

Geisler, S., Holmström, K. M., Skujat, D., Fiesel, F. C., Rothfuss, O. C., Kahle, P. J. and Springer, W. (2010). PINK1/Parkin-mediated mitophagy is dependent on VDAC1 and p62/SQSTM1. *Nat. Cell Biol.* **12**, 119-131.

Gomes, L. C., Di Benedetto, G. and Scorrano, L. (2011). During autophagy mitochondria elongate, are spared from degradation and sustain cell viability. *Nat. Cell Biol.* **13**, 589-598.

Hara-Kuge, S. and Fujiki, Y. (2008). The peroxin Pex14p is involved in LC3-dependent degradation of mammalian peroxisomes. *Exp. Cell Res.* **314**, 3531-3541.

Huang, J., Birmingham, C. L., Shahnazari, S., Shiu, J., Zheng, Y. T., Smith, A. C., Campellone, K. G., Heo, W. D., Gruenheid, S., Meyer, T. et al. (2011). Antibacterial autophagy occurs at PI(3)P-enriched domains of the endoplasmic reticulum and requires Rab1 GTPase. *Autophagy* **7**, 17-26.

Itakura, E. and Mizushima, N. (2011). p62 Targeting to the autophagosome formation site requires self-oligomerization but not LC3 binding. *J. Cell Biol.* **192**, 17-27.

Iwata, J., Ezaki, J., Komatsu, M., Yokota, S., Ueno, T., Tanida, I., Chiba, T., Tanaka, K. and Kominami, E. (2006). Excess peroxisomes are degraded by autophagic machinery in mammals. *J. Biol. Chem.* **281**, 4035-4041.

Johansen, T. and Lamark, T. (2011). Selective autophagy mediated by autophagic adapter proteins. *Autophagy* **7**, 279-296.

Kassmann, C. M. and Nave, K. A. (2008). Oligodendroglial impact on axonal function and survival – a hypothesis. *Curr. Opin. Neurol.* **21**, 235-241.

Kim, P. K., Hailey, D. W., Mullen, R. T. and Lippincott-Schwartz, J. (2008). Ubiquitin signals autophagic degradation of cytosolic proteins and peroxisomes. *Proc. Natl. Acad. Sci. USA* **105**, 20567-20574.

Kirkin, V., Lamark, T., Sou, Y. S., Bjørkøy, G., Nunn, J. L., Bruun, J. A., Shvets, E., McEwan, D. G., Clausen, T. H., Wild, P. et al. (2009a). A role for NBR1 in autophagosomal degradation of ubiquitinated substrates. *Mol. Cell* **33**, 505-516.

Kirkin, V., McEwan, D. G., Novak, I. and Dikic, I. (2009b). A role for ubiquitin in selective autophagy. *Mol. Cell* **34**, 259-269.

Komatsu, M. and Ichimura, Y. (2010). Selective autophagy regulates various cellular functions. *Genes Cells* **15**, 923-933.

Kraft, C., Peter, M. and Hofmann, K. (2010). Selective autophagy: ubiquitin-mediated recognition and beyond. *Nat. Cell Biol.* **12**, 836-841.

Kutateladze, T. G. (2006). Phosphatidylinositol 3-phosphate recognition and membrane docking by the FYVE domain. *Biochim. Biophys. Acta* **1761**, 868-877.

Lamark, T., Perander, M., Outzen, H., Kristiansen, K., Øvervatn, A., Michaelsen, E., Bjørkøy, G. and Johansen, T. (2003). Interaction codes within the family of mammalian Phox and Bem1p domain-containing proteins. *J. Biol. Chem.* **278**, 34568-34581.

Mardakheh, F. K., Auciello, G., Dafforn, T. R., Rappoport, J. Z. and Heath, J. K. (2010). Nbr1 is a novel inhibitor of ligand-mediated receptor tyrosine kinase degradation. *Mol. Cell. Biol.* **30**, 5672-5685.

Meinecke, M., Cizmowski, C., Schliebs, W., Krüger, V., Beck, S., Wagner, R. and Erdmann, R. (2010). The peroxisomal importomer constitutes a large and highly dynamic pore. *Nat. Cell Biol.* **12**, 273-277.

Mitra, K., Wunder, C., Roysam, B., Lin, G. and Lippincott-Schwartz, J. (2009). A hyperfused mitochondrial state achieved at G1-S regulates cyclin E buildup and entry into S phase. *Proc. Natl. Acad. Sci. USA* **106**, 11960-11965.

Mostowy, S., Sancho-Shimizu, V., Hamon, M. A., Simeone, R., Brosch, R., Johansen, T. and Cossart, P. (2011). p62 and NDP52 proteins target intracytosolic Shigella and Listeria to different autophagy pathways. *J. Biol. Chem.* **286**, 26987-26995.

Motley, A. M., Nuttall, J. M. and Hettema, E. H. (2012). Pex3-anchored Atg36 tags peroxisomes for degradation in Saccharomyces cerevisiae. *EMBO J.* **31**, 2852-2868.

Narendra, D., Kane, L. A., Hauser, D. N., Fearnley, I. M. and Youle, R. J. (2010). p62/SQSTM1 is required for Parkin-induced mitochondrial clustering but not mitophagy; VDAC1 is dispensable for both. *Autophagy* **6**, 1090-1106.

Okatsu, K., Saisho, K., Shimanuki, M., Nakada, K., Shitara, H., Sou, Y. S., Kimura, M., Sato, S., Hattori, N., Komatsu, M. et al. (2010). p62/SQSTM1 cooperates with Parkin for perinuclear clustering of depolarized mitochondria. *Genes Cells* **15**, 887-900.

Pankiv, S., Clausen, T. H., Lamark, T., Brech, A., Bruun, J. A., Outzen, H., Øvervatn, A., Bjørkøy, G. and Johansen, T. (2007). p62/SQSTM1 binds directly to Atg8/LC3 to facilitate degradation of ubiquitinated protein aggregates by autophagy. *J. Biol. Chem.* **282**, 24131-24145.

Platta, H. W. and Erdmann, R. (2007). Peroxisomal dynamics. *Trends Cell Biol.* **17**, 474-484.

Platta, H. W., El Magraoui, F., Schlee, D., Grunau, S., Girzalsky, W. and Erdmann, R. (2007). Ubiquitination of the peroxisomal import receptor Pex5p is required for its recycling. *J. Cell Biol.* **177**, 197-204.

Rambold, A. S., Kostelecky, B., Elia, N. and Lippincott-Schwartz, J. (2011). Tubular network formation protects mitochondria from autophagosomal degradation during nutrient starvation. *Proc. Natl. Acad. Sci. USA* **108**, 10190-10195.

Ribeiro, D., Castro, I., Fahimi, H. D. and Schrader, M. (2012). Peroxisome morphology in pathology. *Histol. Histopathol.* **27**, 661-676.

Rizzo, M. A., Springer, G. H., Granada, B. and Piston, D. W. (2004). An improved cyan fluorescent protein variant useful for FRET. *Nat. Biotechnol.* **22**, 445-449.

Singh, I., Singh, A. K. and Contreras, M. A. (2009). Peroxisomal dysfunction in inflammatory childhood white matter disorders: an unexpected contributor to neuropathology. *J. Child Neurol.* **24**, 1147-1157.

Thurston, T. L., Ryzhakov, G., Bloor, S., von Muhlinen, N. and Randow, F. (2009). The TBK1 adaptor and autophagy receptor NDP52 restricts the proliferation of ubiquitin-coated bacteria. *Nat. Immunol.* **10**, 1215-1221.

Till, A., Lakhani, R., Burnett, S. F. and Subramani, S. (2012). Pexophagy: the selective degradation of peroxisomes. *Int. J. Cell Biol.* **2012**, 512721.

Wild, P., Farhan, H., McEwan, D. G., Wagner, S., Rogov, V. V., Brady, N. R., Richter, B., Korac, J., Waidmann, O., Choudhary, C. et al. (2011). Phosphorylation of the autophagy receptor optineurin restricts Salmonella growth. *Science* **333**, 228-233.

Wilson, M. I., Gill, D. J., Perisic, O., Quinn, M. T. and Williams, R. L. (2003). PB1 domain-mediated heterodimerization in NADPH oxidase and signaling complexes of atypical protein kinase C with Par6 and p62. *Mol. Cell* **12**, 39-50.

Zheng, Y. T., Shahnazari, S., Brech, A., Lamark, T., Johansen, T. and Brumell, J. H. (2009). The adaptor protein p62/SQSTM1 targets invading bacteria to the autophagy pathway. *J. Immunol.* **183**, 5909-5916.

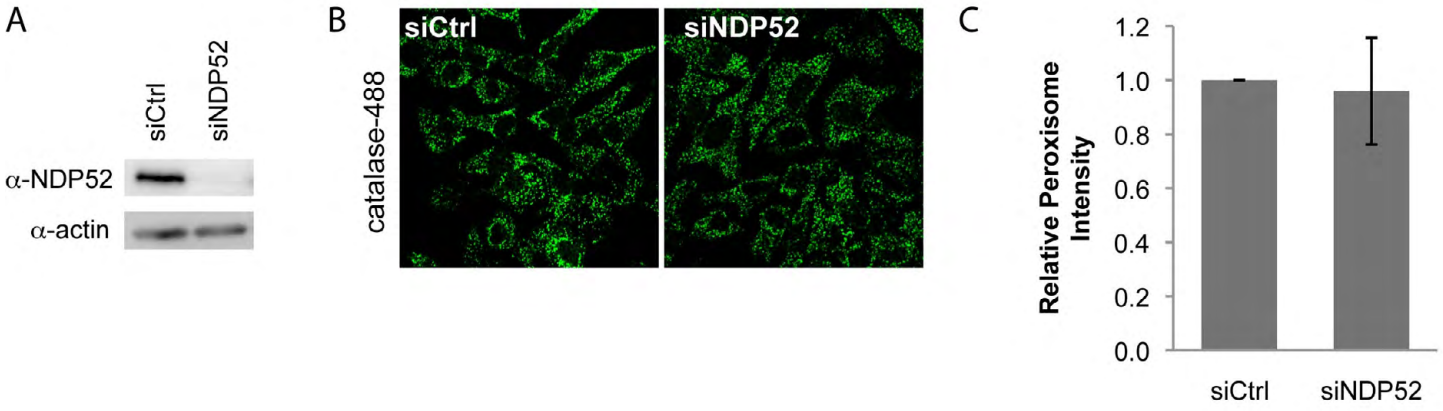

Fig. S1. NDP52 is not required for the endogenous turnover of peroxisomes. HeLa cells treated with non-targeting siRNA (siCtrl) or siRNA against NDP52. **(A)** Immunoblot analysis of cells treated with either control (siCtrl) or NDP52 siRNA (siNDP52) as indicated. The same blot was probed with antibodies against NDP52 and actin. **(B)** Representative immunofluorescence image of HeLa cells probed with anti-Catalase antibody and visualized using AlexaFluor 488 secondary antibody. **(C)** The normalized mean fluorescence intensity of catalase levels in cells treated with control or NDP52 siRNA. siRNA treated cells were fixed and immunostained for endogenous catalase. The mean catalase fluorescence intensity of at least 100 cells was measured for both control siRNA and NDP52 siRNA. The average of three independent sets of experiments normalized against the control non-targeting siRNA (siCtrl) is shown in the bar graph. Error bars represent the standard deviation.

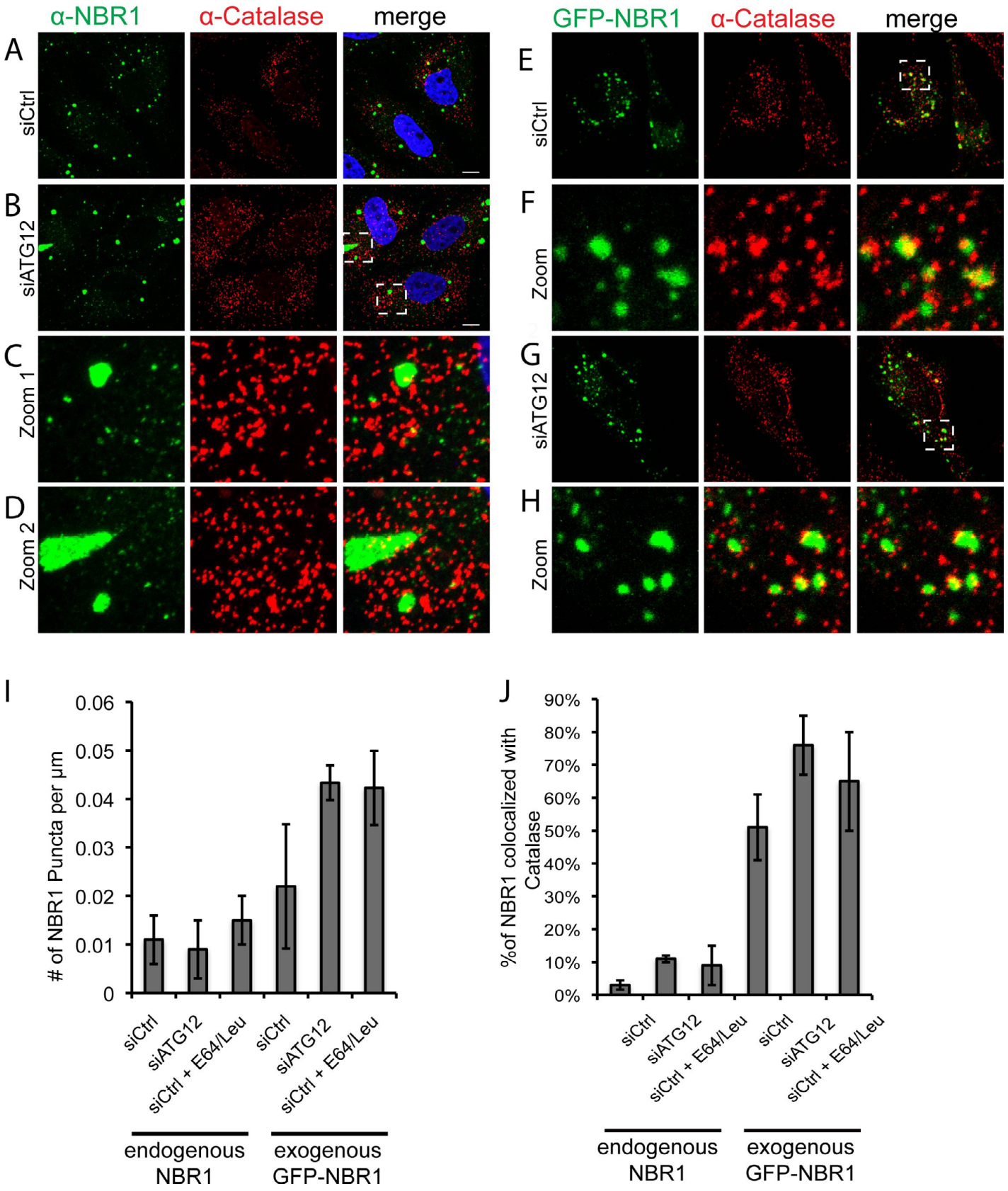

Fig. S2. NBR1/peroxisome cluster formation is dependent on NBR1 expression levels. HeLa cells treated with either non-targeting siRNA (siCtrl) **(A)**, or siRNA against ATG12 (siATG12) **(B)** were treated with lysosomal protease inhibitors E-64 and leupeptin. They were fixed and immunostained for endogenous NBR1 and catalase. **(C-D)** enlargement of the regions outlined by the box in (B). **(E-H)** HeLa cells treated with either siCtrl or siATG12 were transfected with Cherry-NBR1 and Lamp1-GFP, and treated with lysosomal protease inhibitors E-64 and leupeptin. Also shown is the magnification of the white box in the merge. **(I)** Quantification of the number of NBR1 punctate structures in cells treated with either siCtrl or siATG12. As indicated some were also treated with E64/leupeptin. Both endogenous NBR1 and exogenously expressed GFP-NBR1 quantifications are shown. **(J)** Quantification of the % of NBR1 colocalized with catalase. Scale bars, 10 µm.

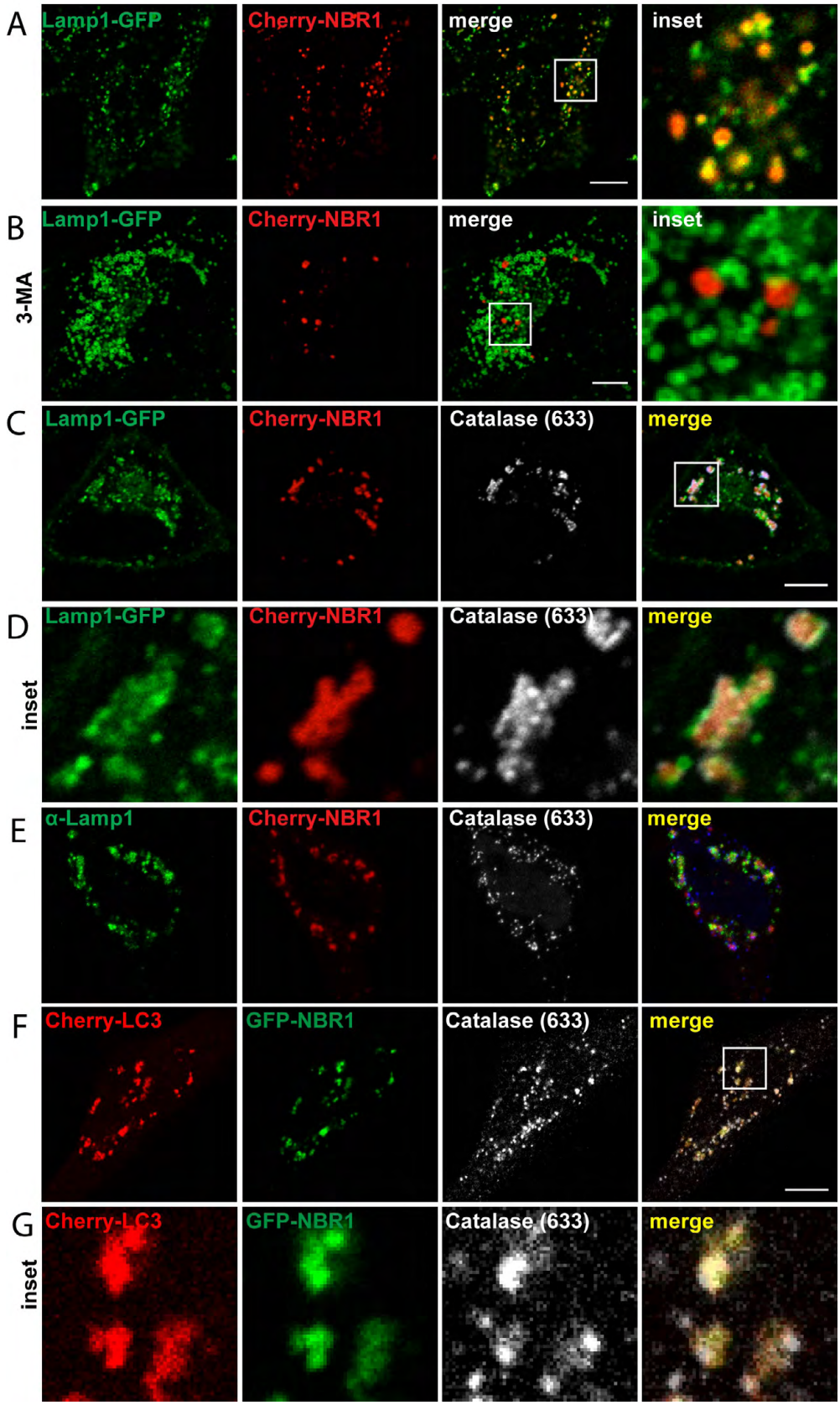

Fig. S3. NBR1/peroxisome clusters are localized to lysosomes. (A) HeLa cells transfected with Cherry-NBR1 and Lamp1-GFP, and treated with lysosomal protease inhibitors E-64 and leupeptin. Also shown is the magnification of the white box in the merge. **(B)** Same as (A) except the cells were also treated with 3-MA. **(C)** HeLa cells were transfected with Cherry-NBR1 and Lamp1-GFP, and treated with lysosomal inhibitors. The cells were fixed and immunostained for endogenous catalase. **(D)** Magnification of an area in (C) indicated by the white box. **(E)** HeLa cells expressing Cherry-NBR1 and treated as in (A) were fixed and probed for endogeneous NBR1 and catalase. **(F)** HeLa cells expressing Cherry-LC3 and GFP-NBR1 were fixed and immunostained for endogenous catalase. **(G)** Magnification of the area in (E) indicated by the white box. Scale bars, 10 μm.

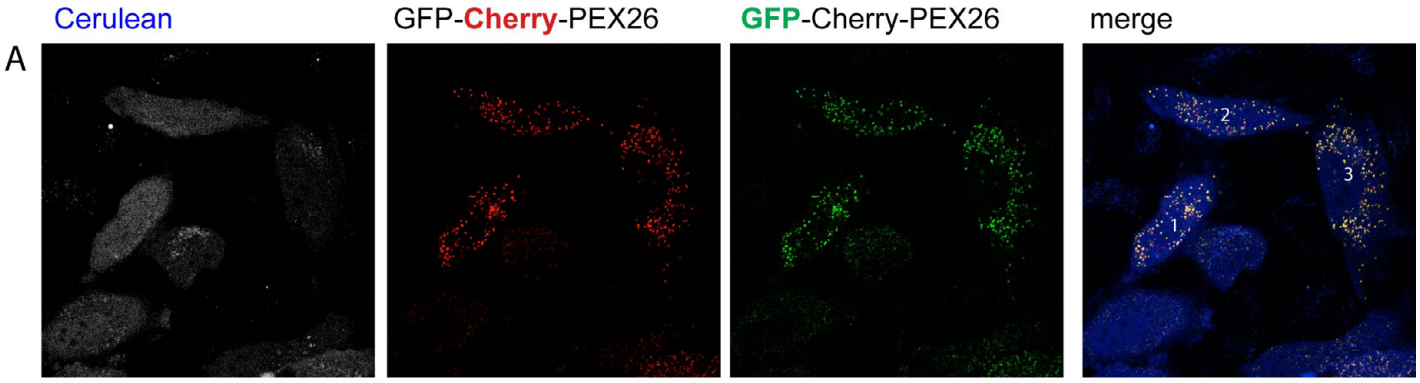

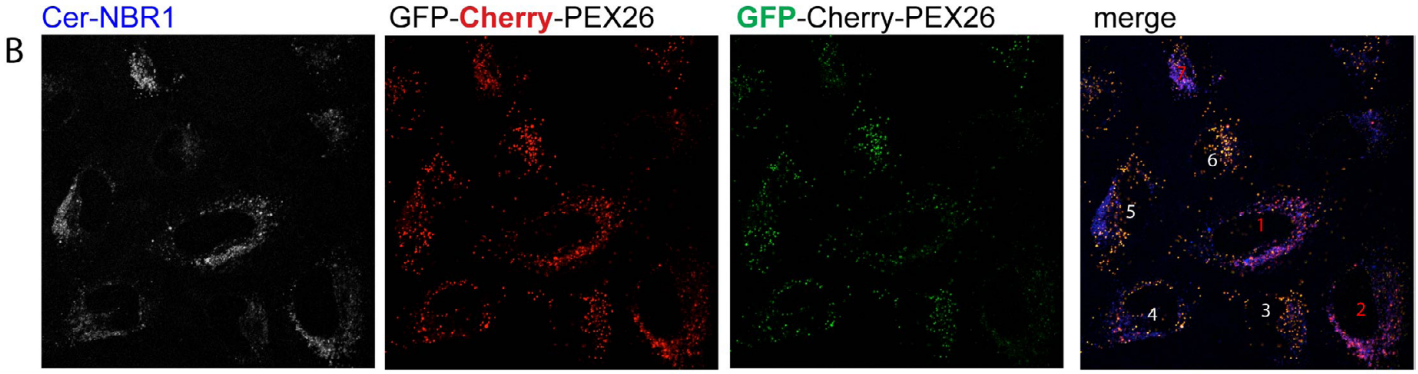

C

	Total Pixel with RED	Total Pixel RED ONLY(where red is 3X>green)	% of Red only Pixel	Pexophagy induced cell (>20%)
Cer Cell 1	822	0	0.0%	-
Cer Cell 2	809	0	0.0%	-
Cer Cell 3	530	0	0.0%	-
NBR1 Cell 1	2628	1487	56.6%	✓
NBR1 Cell 2	5137	3540	68.9%	✓
NBR1 Cell 3	2155	41	1.9%	-
NBR1 Cell 4	2155	345	16.0%	-
NBR1 Cell 5	3313	87	2.6%	-
NBR1 Cell 6	2417	6	0.2%	-
NBR1 Cell 7	2579	1986	77.0%	✓

Fig. S4. RG-Lysosome assay for Pexophagy using GFP-Cherry-PEX26. Representative example of cells transfected with GFP-Cherry-PEX26$_{TM}$ and Cerulean **(A)** or Cerulean-NBR1 **(B)**, and treated with lysosomal inhibitors Leupeptin and E-64. The presence of red-only peroxisomes indicates pexophagy. In the merge images Cerulean constructs are shown in blue. **(C)** Example of the quantification of pexophagy, as discussed in Materials and Methods. The cells are numbers in the merge images in (A) and (B). Cells with more than 20% of Red only pixels compare to the total red pixels are considered to have increased pexophagy (indicated with a 'check-mark')

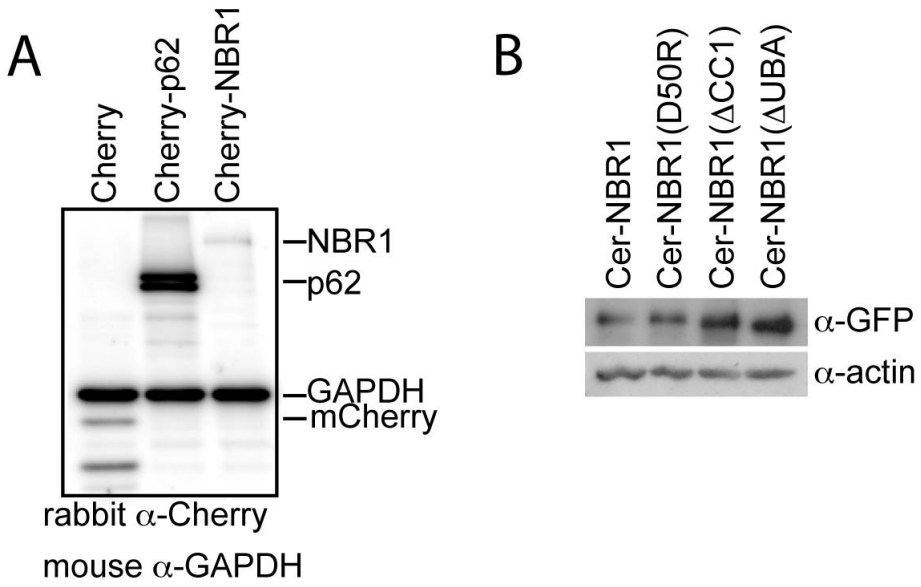

Fig. S5. Expression levels of Cer-NBR1 and mutants. (A) Immunoblot of lysates of HeLa cells transiently transfected with Cherry, Cherry-p62, Cherry-NBR1 probed with Rabbit anti-Cherry and mouse anti-GAPDH. **(B)** Cer-NBR1 and its various mutants were analyzed by SDS-PAGE and immunoblotted with anti-GFP antibody and anti-actin.

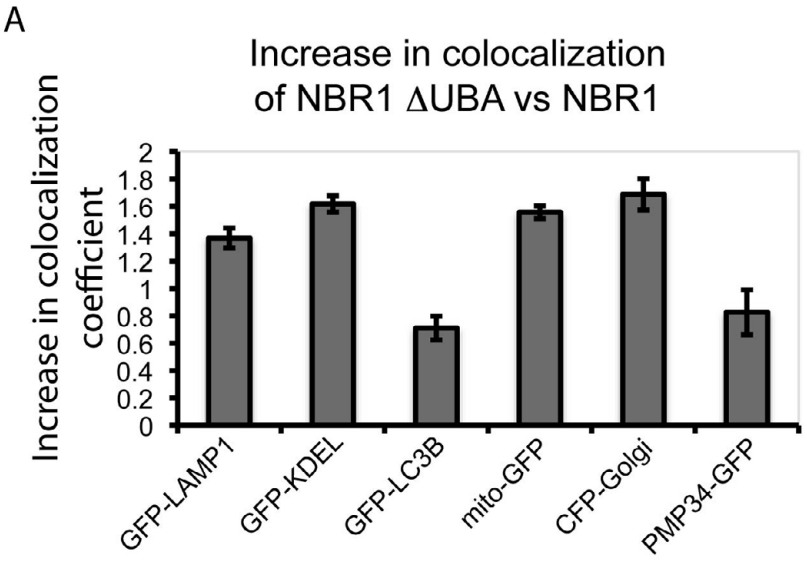

B

p-values of the difference between NBR1 and NBR1-ΔUBA with various organelle markers

GFP-Lamp1 (lysosomes)	0.018
GFP-KDEL (ER)	2.91E-07
GFP-LC3B (autophagosome)	1.43E-08
GFP-mito (mitochondria)	6.25E-10
CFP-Golgi (Golgi Apparatus)	0.046
PMP34-GFP * (peroxisomes)	0.16

* Not significantly different (p>0.05)

Fig. S6. The increase in colocalization of NBR1 JΔUBA with various organelles relative to wild type NBR1. HeLa cells were co-transfected with either wild type NBR1 or NBR1 JΔUBA with various organelle markers as shown. **(A)** The fraction of NBR1 or NBR1 JΔUBA colocalized with the specific organelle markers was determined using Mander's colocalization coefficient. The change in colocalization of NBR1 JΔUBA versus wild type NBR1 is shown. The change in colocalization is the ratio of the colocalization coefficient of NBR1 JΔUBA over that of the wild type. **(B)** the p-value of the difference in the colocalization coefficient between NBR1 ΔUBA and NBR1. Box shaded in blue indicates no significant difference.

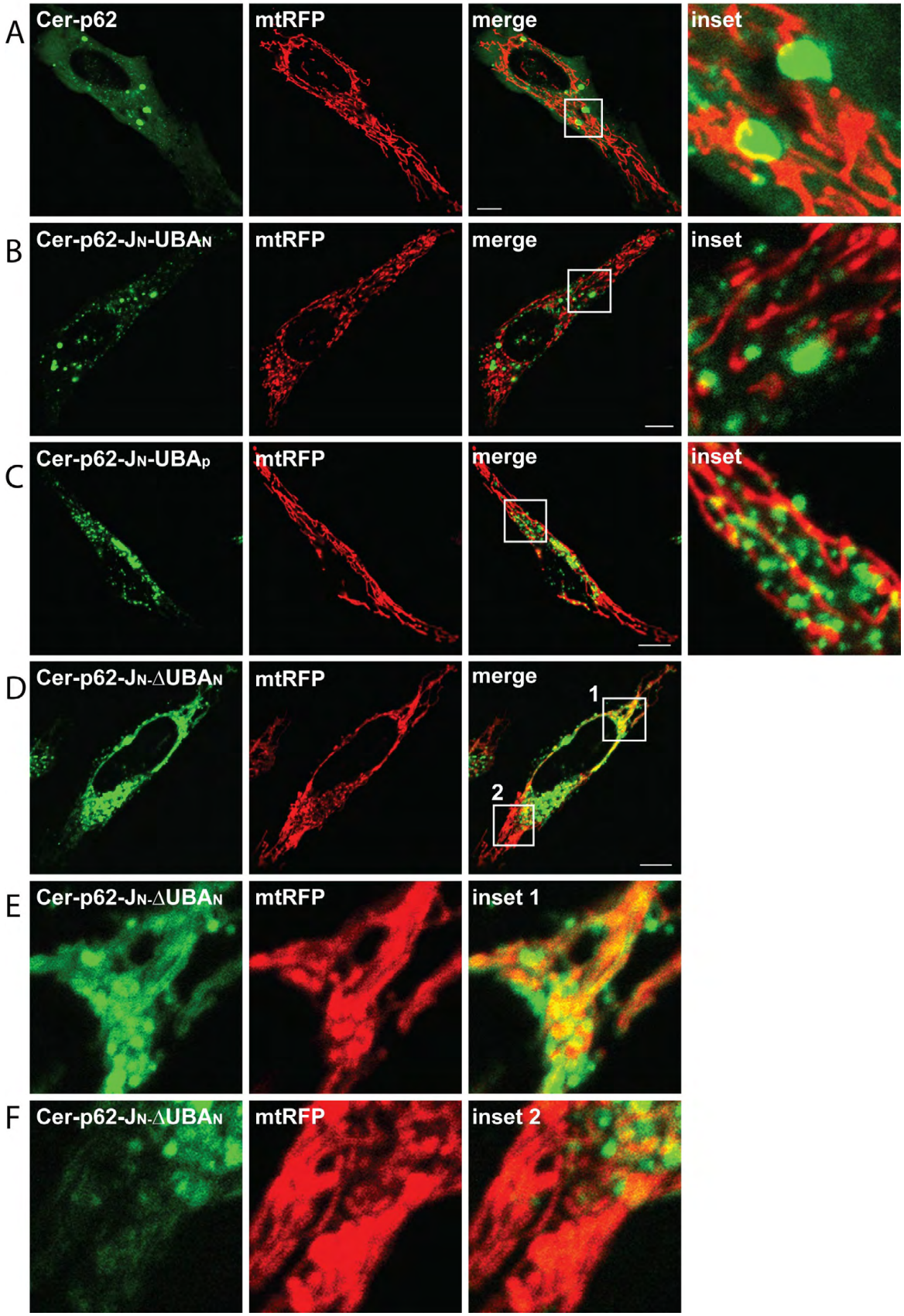

Fig. S7. HeLa cells were co-transfected with mitochondrial-targeting red fluorescent protein (mtRFP) and **(A)** Cerulean-p62, **(B)** Cer-p62-JN-UBA$_N$, **(C)** Cer-p62-J$_N$-UBA$_p$, or **(D)** Cer-p62-J$_N$-ΔUBA for 16 hours. The cells were imaged live. The white box area is magnified in the frame labeled 'inset'. Two insets were shown in the cell expressing mtRFP and Cer-p62-J$_N$-ΔUBA (D), which are shown in **(E)** inset 1 and **(F)** inset 2.

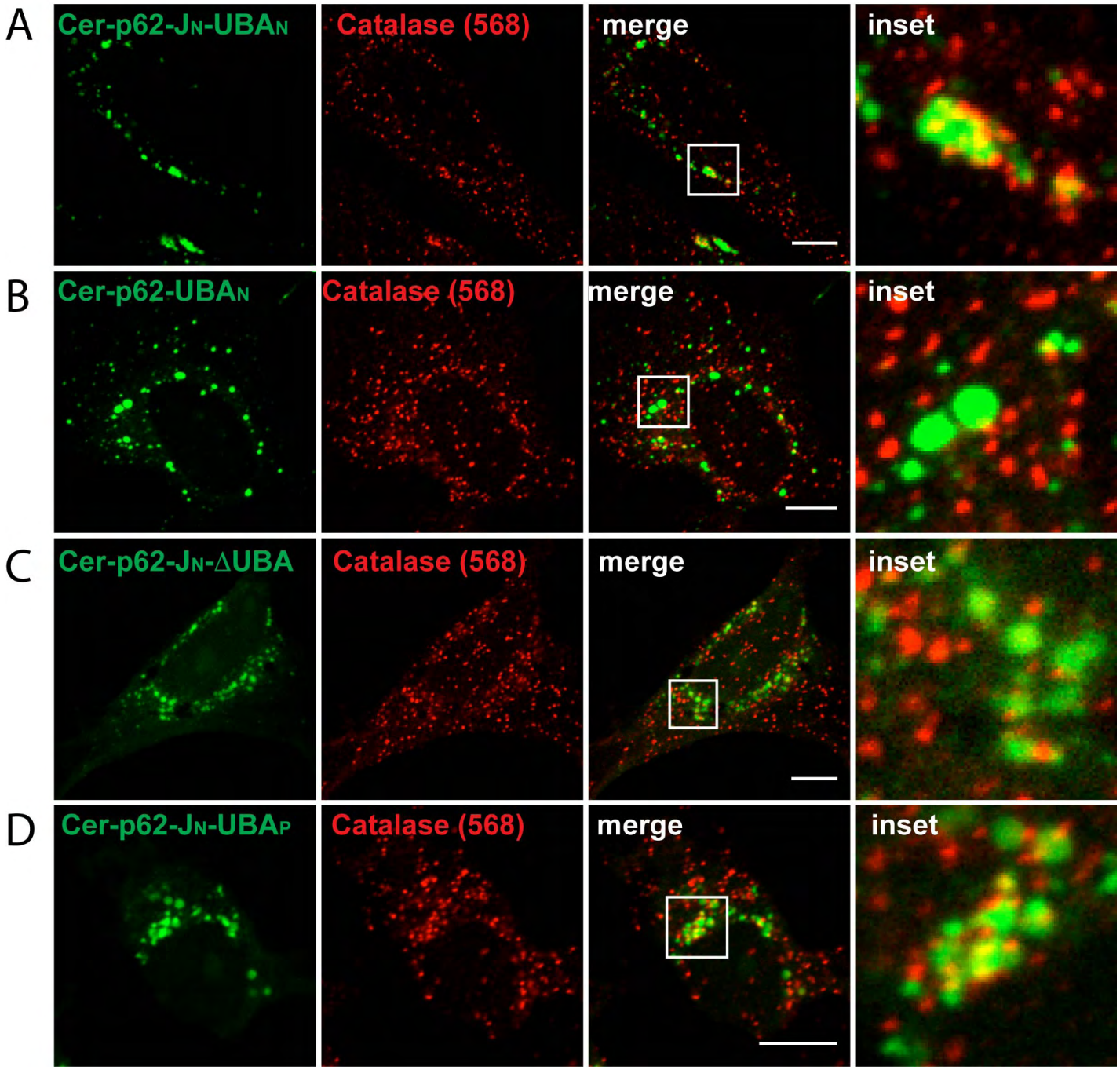

Fig. S8. Representative images of HeLa cells transfected with (**A**) p62 with the J and UBA domain of NBR1 (Cer-p62-J_N-UBA_N); (**B**) p62 with only the UBA domain of NBR1 (Cer-p62-UBA_N); (**C**) p62 with only the J domain and no UBA (Cer-p62-J-ΔUBA); or (**D**) p62 with NBR1 J domain and its own UBA domain (Cer-p62-J_N-UBA_p). Cells were fixed and immunostained for catalase. Scale bars, 10 μm.

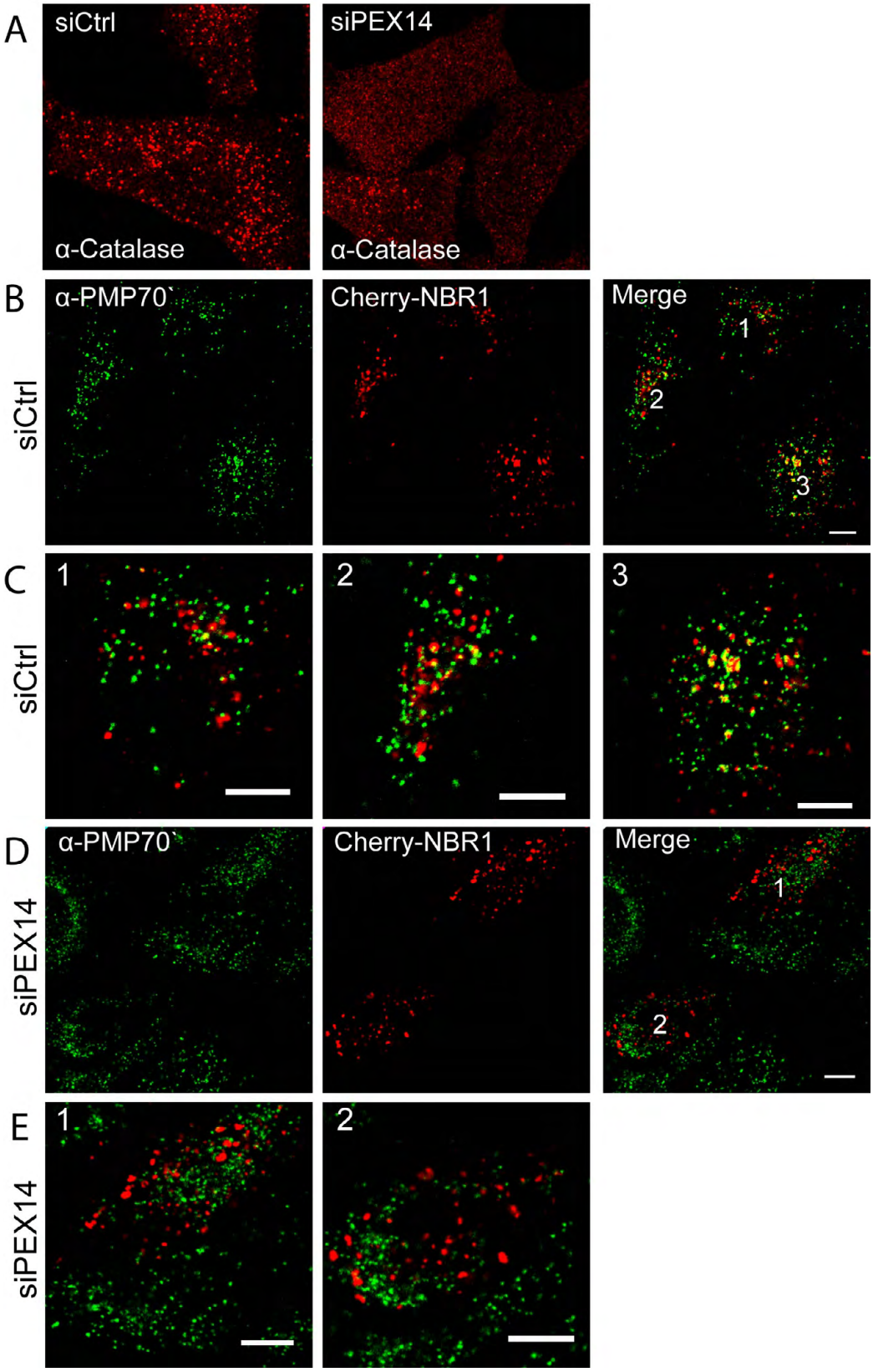

Fig. S9. Representative images of HeLa cells treated with siRNA against PEX14. **(A)** Cells treated with either control siRNA (siCtrl) or siRNA against PEX14 (siPEX14) immunostained for catalase. The siPEX14 consist of two siRNA sequences: (1) 5'-GGCAGGCAUUGCAUUUTT-3' and (2) 5'-GAACUCAAGUCCGAAAUUTT-3'. Note the increase in cytosolic localization of catalase in siPEX14 treated cells. **(B)** siCtrl treated cells expressing Cherry-NBR1 immunostained for PMP70. **(C)** Magnification of cells in (B). Cells 2 and 3 show NBR1/PMP70 clustering. **(D)** siPEX14 treated cells transiently expressing Cherry-NBR1 were immunostained for PMP70. **(E)** Magnification of cells in (D).

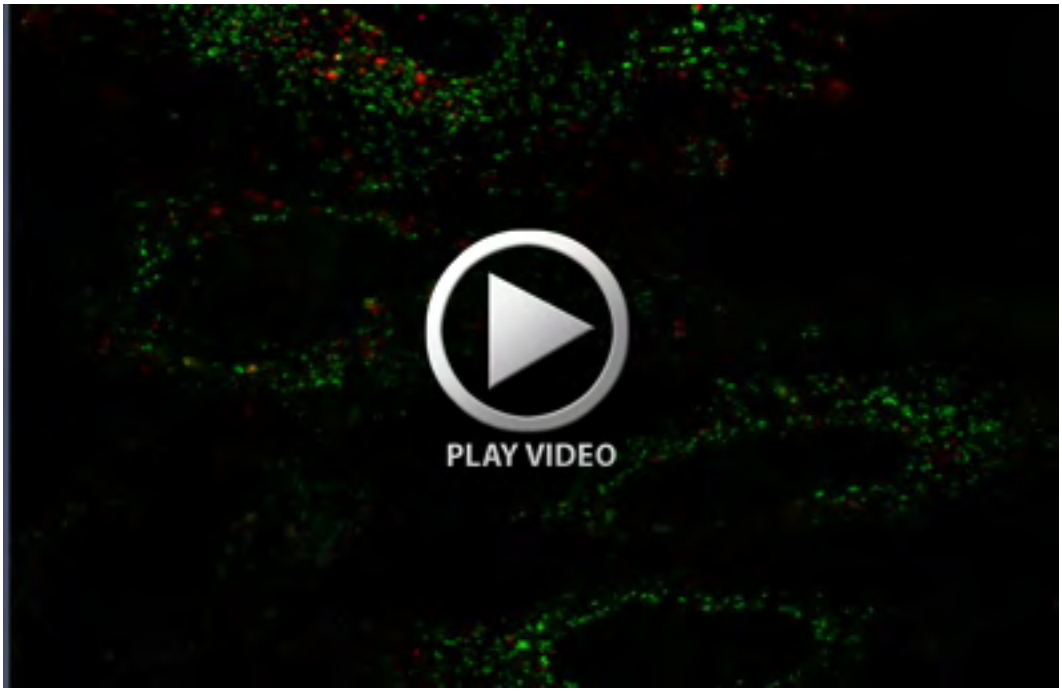

Movie 1. Time-lapse imaging of a HeLa cell expressing Cherry-NBR1 and PMP34-GFP. Images were acquired 16 hours after transfection at 2 hour intervals for 14 hours. Images were compiled using Zeiss Zen software.

Movie 2. Time-lapse imaging of a HeLa cell expressing Cer-NBR1 and GFP-Cherry-PEX26$_{TM}$. Images were acquired every hour for 48 hours. Images were compiled using Zeiss Zen software and Adobe Photoshop.